1961

Analysis of a Vertically Rising Vehicle

Sheldon Baron
College of William & Mary - Arts & Sciences

ANALYSIS OF A VERTICALLY RISING VEHICLE

A Thesis

Presented to

The Faculty of the Department of Physics

The College of William and Mary in Virginia

In Partial Fulfillment

Of the Requirements for the Degree of

Master of Arts

By

Sheldon Baron

June 1961

APPROVAL SHEET

This thesis is submitted in partial fulfillment of

the requirements for the degree of

Master of Arts

Sheldon Baron

Author

Approved, June 1961:

D. G. McLennan

H. MacKnight

James D. Lawrence, Jr.

Melvin K. Pittman

ACKNOWLEDGMENTS

The writer wishes to express his appreciation to the staff of the Physics Department of William and Mary for their guidance and criticism. The author is indebted to Homer G. Morgan of the Langley Research Center, NASA, whose contributions made this paper possible and to Mr. Charles N. Valade, also of LRC, for his cooperation. The many kindnesses of the Langley Training office and the typing talents of Mrs. Leona Harris were invaluable in the preparation of this paper.

TABLE OF CONTENTS

LIST OF TABLES

LIST OF FIGURES

Figure

ABSTRACT

An analytical investigation of the loads and responses of a simplified elastic rocket vehicle flying a vertical trajectory has been conducted. The external forces assumed acting on the rocket were produced by a series of wind shear reversals and several measured wind profiles. The system was described by three rigid-body modes and three elastic modes, and was stabilized by a simplified control function. The differential equations had time-dependent coefficients and were solved on an analog computer.

Time-dependent coefficients of the differential equations were found to be necessary to predict loads when the wave length of the wind shear reversal became sufficiently long. Errors which would result from using time-fixed coefficients were shown to depend on, among other factors, the ratio of bending frequency to control frequency, the thrust-to-weight ratio, and the control system of the rocket.

Detailed wind profiles measured by a smoke-trail technique were generally found to produce larger loads on the rocket than wind profiles measured by balloon-sounding techniques. These differences were as large as 15 to 20 percent, depending on the parameters of the system. It was noted that the character of the bending-moment response to these profiles, whether primarily inertial or aerodynamic, and the magnitude of bending mode excitation, depended on the type of control system as well as the rocket's thrust-to-weight ratio and bending-mode frequency to control frequency ratio.

TABLE I

LIST OF SYMBOLS

$a_i, i = 1,2,3$	characteristic values of a uniform beam with free-free boundary conditions
B.M.	bending moment, ft-lb
C_{ij}	generalized aerodynamic coefficients appearing in equation (6a)
D_m, D_{nj}	constants appearing in bending-moment equation
EI	stiffness constant of a uniform beam, lb-ft^2
F_{xA}, F_{yA}	components of aerodynamic force in body axes, lb
F_{xE}, F_{yE}	components of engine force in body axes, lb
g	gravitational constant, ft/sec^2
h	altitude, ft
h_o	initial altitude, ft
I_{sp}	specific impulse of rocket, sec
K_1, K_2, K_3	gain constants of the control function, equation (2)
L	length of the rocket, ft
l_e	distance from c.g. to aft end of vehicle, ft
M	mass of the rocket at any instant, lb-sec^2/ft
M_o	lift-off mass of the rocket, lb-sec^2/ft
M_{zA}	aerodynamic pitching moment, lb-ft
M_{zE}	pitching moment due to engine, lb-ft
$\bar{q}_i, i = 1,2,3$	generalized coordinate of ith mode, divided by L, nondimensional

Q_{iA}	generalized aerodynamic force, lb
Q_{iE}	generalized engine force, lb
S_o	base area of the vehicle, ft^2
t	time, sec
T	thrust, lb
$u_e(x,t)$	elastic deflection at aft end of vehicle, ft
V_m	velocity of the rocket, ft/sec
V	velocity of rocket relative to air, ft/sec
V_w	horizontal velocity of wind, ft/sec
W_o	lift-off weight of rocket, lb
$\dot{x}_c,\dot{y}_o$	center-of-gravity velocity of rocket in body axes, divided by L, per sec
$\bar{x}$	distance along rocket elastic axis, measured from aft end, divided by L, nondimensional
$\bar{x}_n$	distance from aft end to nth station, divided by L, nondimensional
α	angle of attack, radians
α'	total angle of attack relative to the air stream, radians
α_w	angle of attack due to wind, radians
$\bar{\gamma}$	angle between vertical reference and inertial velocity vector, radians
δ	angle of deflection of thrust vector from rocket center line, radians
$\bar{\theta}$	angle between vertical reference and body axis, radians
Λ	wave length of input wind, ft
ξ_p	damping ratio of rigid-body pitch mode, dimensionless
ρ	density of atmosphere, $lb\text{-}sec^2/ft^4$
ρ_o	density of atmosphere at sea level, $lb\text{-}sec^2/ft^4$

$\omega_i, i = 1,2,3$	natural frequency of ith mode, radians/sec
ω_p	natural frequency of pitch mode, radians/sec

A dot indicates a differentiation with respect to time.

A prime indicates a differentiation with respect to x (unless specifically noted otherwise).

ANALYSIS OF A VERTICALLY RISING VEHICLE

INTRODUCTION

The analysis and design of space vehicles is a subject which occupies a prominent position in physics and engineering. The stability of such vehicles and the loads which they experience are a prime consideration in their design.

A general analysis of any specific physical system includes direct experimentation, experimentation with scale models, experimentation with analog models, and several mathematical techniques[1]. This paper is concerned with the application of the last two methods of analysis, experimentation with analog models and mathematical techniques, as applied to the study of loads on a space vehicle.

An exact analytical model of a space vehicle would require a set of nonlinear differential equations to describe both the rigid and elastic degrees of freedom. Since the mass of the vehicle changes as fuel is consumed, these equations would necessarily have varying coefficients. A description of the external forces, such as the motion of the atmosphere, would be necessary as forcing functions for the differential equations.

However, the availability of certain types of atmospheric data, and the desire to simplify the analytical and computational procedures, have resulted in approximations to the exact analytical model. An essential feature of most of these approximate analytical approaches is the use of a constant-coefficient analysis when considering the space vehicle as an elastic body.

This investigation will attempt to determine what, if any, significant differences may be introduced by using the constant-coefficient analysis as opposed to the more realistic variable-coefficient approach. The response of the variable-coefficient, elastic model to several experimental wind profiles is also investigated. The effect of some of the more important physical parameters is studied. Brief mention is made of some other analytical techniques which may be applied to the loads analysis of space vehicles.

REFERENCES FOR INTRODUCTION

[1]Rogers, A. E., and Connolly, T. N. Analog Computation in Engineering Design. McGraw-Hill Book Co., Inc., 1960.

CHAPTER I

ANALYSIS

The analysis of a physical system requires a complete description of the physical system, the derivation of a set of differential equations to represent the system and a method for obtaining the solution of these equations.

Physical System

For this study the space vehicle is considered to be restricted to motion in a plane. The vehicle is assumed to be flying vertically through horizontal winds and angular deviations from the vertical flight path are assumed small. The mass of the vehicle is uniformly distributed and the change in mass is assumed to occur in a uniform manner over the length of the vehicle, similar to the situation to be expected on a solid propelled single-stage vehicle. Both the rate of change of mass and the specific impulse of the rocket are assumed constant, and therefore, the motor produces constant thrust.

The vehicle is an unfinned parabolic body of revolution, resulting in an aerodynamically unstable configuration. The aerodynamic coefficients are determined by momentum or "slender-body" theory (appendix A).

The vehicle is stabilized by rotating a gimballed engine and thus deflecting the thrust vector. The engine is assumed to respond instantaneously to the control system command. As a matter of interest, since previous studies have shown significant differences in response when using attitude or angle-of-attack control, parallel studies using both systems were made. However, no effort is made to optimize either control system and therefore, no comparison of their relative merits is justified.

The response of the vehicle will be examined by consideration of the bending moment. This variable is chosen because it gives an excellent indication of the over-all response and because of its physical importance as a measure of the loads acting on the vehicle. The responses will be calculated for an altitude range from 20,000 ft to 40,000 ft.

The responses and loads for an actual space vehicle would certainly be influenced by the factors which are neglected in arriving at this model of the system. However, the model retains the essential features required to study the particular effects considered. It is believed that the simplifications may actually serve to clarify some aspects of the loads problem.

Equations of Motion

The equations of motion are written in a right-handed body axis coordinate system illustrated in figure 1. The equations of motion in moving coordinates for a flexible missile can be written using modified Lagrange's equations.

Assuming that the elastic deflection can be represented by a summation of normal modes

$$u(x,t) = \sum_{i} \varphi_i(x) q_i(t)$$

the kinetic and potential energies can be written

$$\text{Kinetic energy} = \frac{1}{2} M(\dot{x}_o^2 + \dot{y}_o^2) + \frac{1}{2} I\dot{\theta}^2 + \frac{1}{2} \sum_i M_i\dot{q}_i^2$$

$$\text{Potential energy} = \frac{1}{2} \sum_i \omega_i^2 M_i q_i^2$$

where,

$$M_i = \int_o^L m(x)\left[\varphi_i(x)\right]^2 dx$$

$\omega_i \equiv$ frequency of the ith normal mode

The Lagrangian, L,' is then given by

$$L' = \frac{1}{2} M(\dot{x}_o^2 + \dot{y}_o^2) + \frac{1}{2} I\dot{\theta}^2 + \frac{1}{2} \sum_i M_i\dot{q}_i^2 - \frac{1}{2} \sum_i \omega_i^2 M_i q_i^2$$

Substituting this expression in Lagrange's equations for moving coordinates[2]

$$\frac{d}{dt}\frac{\partial L'}{\partial \dot{x}_o} - \dot{\theta}\frac{\partial L}{\partial \dot{y}_o} = \sum F_x$$

$$\frac{d}{dt}\frac{\partial L'}{\partial \dot{y}_o} + \dot{\theta}\frac{\partial L}{\partial \dot{x}_o} = \sum F_y$$

$$\frac{d}{dt}\frac{\partial L'}{\partial \dot{\theta}} + \dot{x}_o\frac{\partial L}{\partial \dot{y}_o} - \dot{y}_o\frac{\partial L}{\partial \dot{x}_o} = \sum M_z$$

$$\frac{d}{dt}\frac{\partial L'}{\partial \dot{q}_i} - \frac{\partial L}{\partial q_i} = \sum Q_i$$

and performing the indicated operations yields

$$M\ddot{x}_o + \dot{M}\dot{x}_o - M\dot{\theta}\dot{y}_o = \sum F_x$$

$$M\ddot{y}_o + \dot{M}\dot{y}_o + M\dot{\theta}\dot{x}_o = \sum F_y$$

$$I\ddot{\theta} + \dot{I}\dot{\theta} = \sum M_z$$

$$M_i\ddot{q}_i + \dot{M}_i\dot{q}_i + M_i\omega_i^2 q_i = \sum Q_i \qquad (1)$$

The forces and moments which are considered as acting on the body are those produced by the engine (referred to as jet forces and moments), aerodynamic forces and moments, and gravity.

$$\sum F_x = F_{xE} + F_{xA} - Mg \sin \theta$$

$$\sum F_y = F_{yE} + F_{yA} - Mg \cos \theta$$

$$\sum M_z = M_{zE} + M_{zA}$$

$$\sum Q_i = Q_{iE} + Q_{iA}$$

Substituting the expressions for the jet forces and moments obtained in appendix B, in equations (1) yields

$$M\ddot{x}_o - M\dot{\theta}\dot{y}_o = T - Mg \sin\theta + F_{xA}$$

$$M\ddot{y}_o + M\dot{\theta}\dot{x}_o = \dot{M}\left[-l_e\dot{\theta} + \sum_j \varphi_j(0)\dot{q}_j(t)\right] + T\left[\delta + \sum_j \varphi_j'(0)q_j(t)\right]$$
$$- Mg\cos\theta + F_{yA}$$

$$I\ddot{\theta} + \dot{I}\dot{\theta} = \dot{M}\left[l_e^2\dot{\theta} - l_e \sum_j \varphi_j(0)\dot{q}_j(t)\right] - T\left[l_e\left(\delta + \sum_j \varphi_j'(0)q_j(t)\right)\right.$$
$$\left. + \sum_j \varphi_j(0)q_j(t)\right] + M_{zA}$$

$$M_i\ddot{q}_i + \dot{M}_i\dot{q}_i = \dot{M}\varphi_i(0)\left[\dot{y}_o - l_e\dot{\theta} + \sum_j \varphi_j(0)\dot{q}_j(t)\right] + T\varphi_i(0)\left[\delta + \sum_j \varphi_j'(0)q_j(t)\right]$$
$$+ Q_{iA} - M_i\omega_i^2 q_i \qquad (2)$$

Letting

$$x = \frac{x}{L},\ \bar{x}_o = \frac{x_o}{L},\quad \bar{y}_o = \frac{y_o}{L},\quad \bar{q}_i = \frac{q_i}{L},\ I = K^2M,\quad \frac{T}{ML} = \frac{T}{W_o}\frac{g}{L}\frac{M_o}{M},\quad \text{and}$$

$$M_i = ML \int_o^1 \frac{m(\bar{x})}{M}\left[\varphi_i(\bar{x})\right]^2 d\bar{x} = MA_i$$

and assuming k and Ai to be constant in time, we obtain

$$\ddot{x}_o - \dot{\theta}\dot{y}_o = \frac{T}{W_o}\ \frac{g}{L}\frac{M_o}{M} - \frac{g}{L}\sin\theta + \frac{F_{xA}}{ML}$$

$$\ddot{y}_o + \dot{\theta}\dot{x}_o = \frac{\dot{M}}{M}\left[-\frac{l_e}{L}\dot{\theta} + \sum_j \varphi_j(0)\dot{\bar{q}}_j(t)\right] + \frac{T}{W_o}\frac{g}{L}\ \frac{M_o}{M}\left[\delta + \sum_j \varphi_j{}'(0)\bar{q}_j(t)\right]$$
$$- \frac{g}{L}\cos\theta + \frac{F_{yA}}{ML}$$

$$\frac{k}{L}^2\ddot{\theta} + \frac{\dot{M}}{M}\frac{k}{L}^2\dot{\theta} = \frac{\dot{M}}{M}\left[\left(\frac{l_e}{L}\right)^2\dot{\theta} - \frac{l_e}{L}\ \sum_j \varphi_j(0)\dot{\bar{q}}_j(t)\right] - \frac{T}{W_o}\frac{g}{L}\frac{M_o}{M}\left[\frac{l_e}{L}\left(\delta\right.\right.$$
$$\left.\left. + \sum_j \varphi_j{}'(0)\bar{q}_j(t)\right) + \sum_j \varphi_j(0)\bar{q}_j(t)\right] + \frac{M_{zA}}{ML^2}$$

$$A_i\ddot{\bar{q}}_i + \frac{\dot{M}}{M}A_i\dot{\bar{q}}_i = \frac{\dot{M}}{M}\varphi_i(0)\left[\dot{y}_o - \frac{l_e}{L}\dot{\theta} + \sum_j \varphi_j(0)\dot{\bar{q}}_j(t)\right]$$
$$+ \frac{T}{W_o}\ \frac{g}{L}\ \frac{M_o}{M}\varphi_i(0)\left[\delta + \sum_j \varphi_j{}'(0)q_j(t)\right] + \frac{Q_{iA}}{ML}$$
$$+ A_i\bar{q}_i(a_i)\ \frac{EI}{M_oL^3}\ \frac{\dot{M}}{M}\ \frac{I_{sp}}{T/W_o} \qquad (3)$$

Since for a uniform mass distribution the frequency, ω_i^2, can be written[3]

$$\omega_i^2 = a_i\frac{EI}{M_oL^3}\ \frac{M_o}{\dot{M}}\ \frac{\dot{M}}{M} = -a_i\frac{EI}{M_oL^3}\ \frac{I_{sp}}{T/W_o}\frac{\dot{M}}{M}$$

and we have a linear mass variation and a constant specific impulse from the engine so that

$$M = M_o + \dot{M}t$$

and

$$T = -gI_{sp}\dot{M}$$

then

$$\frac{M_o}{M} = \frac{M_o}{\dot{M}} \frac{\dot{M}}{M} = - \frac{W_o/g}{T/g\ I_{sp}} \frac{\dot{M}}{M} = - \frac{I_{sp}}{T/W_o} \frac{\dot{M}}{M}$$

and

$$\frac{\dot{M}}{M} = \frac{1}{\frac{M_o}{\dot{M}} + t} = \frac{1}{t - I_{sp}/T/W_o}$$

Substituting the aerodynamic forces and moments obtained in appendix A, and the constants for a uniform beam obtained in appendix C, the equations of motion may be written

$$\ddot{x}_o - \dot{\theta}\dot{y}_o = - \frac{g}{L} I_{sp} \frac{\dot{M}}{M} - \frac{g}{L}$$

$$\ddot{y}_o + \dot{\theta}\dot{x}_o = \frac{\dot{M}}{M}\left[- \frac{1}{2}\dot{\theta} + \sum_j \dot{q}_j\right] - \frac{g}{L} I_{sp} \frac{\dot{M}}{M}\left[\delta - 4.647\ \bar{q}_1 - 7.859\ \bar{q}_2 - 11.0\ \bar{q}_3\right]$$

$$- \frac{g}{L}\bar{\theta} - \frac{\rho_o S_o L}{M_o} \frac{\rho}{\rho_o} \frac{I_{sp}}{T/W_o} \frac{\dot{M}}{M}\left[\frac{V}{L}^2 \alpha + \frac{V}{L}\left(\frac{1}{2}\dot{\theta} + \frac{8}{15}\dot{\alpha}\right)\right]$$

$$\ddot{\theta} = \frac{\dot{M}}{M}\left[2\dot{\theta} - 6\sum_j \dot{q}_j\right] + 6\frac{g}{L} I_{sp} \frac{\dot{M}}{M}\left[\delta - 4.647\ \bar{q}_1 - 7.859\ \bar{q}_2 - 11.0\ \bar{q}_3\right]$$

$$+ 12\frac{g}{L} I_{sp} \frac{\dot{M}}{M}\sum_j q_j - \frac{\rho_o S_o L}{M_o} \frac{\rho}{\rho_o} \frac{I_{sp}}{T/W_o}\left[\frac{V}{L}^2 \frac{1}{30}\alpha + \frac{V}{L}\left(- \frac{3}{20}\theta - \frac{1}{10}\dot{\alpha}\right)\right]$$

$$\ddot{q}_i + \frac{\dot{M}}{M}\dot{q}_i - \frac{I_{sp}}{T/W_o}\frac{\dot{M}}{M} e_i \frac{EI}{M_o L^3}\bar{q}_i = 4\frac{\dot{M}}{M}\left[\dot{y}_o - \frac{1}{2}\dot{\theta} + \sum_i \dot{q}_j(t)\right] - 4\frac{g}{L} I_{sp} \frac{\dot{M}}{M}\left[\delta\right.$$

$$\left. - 4.647\ \bar{q}_1 - 7.859\ \bar{q}_2 - 11.0\ \bar{q}_3\right]$$

$$- 4\frac{\rho_o S_o L}{M_o} \frac{\rho}{\rho_o} \frac{I_{sp}}{T/W_o}\left[\frac{V}{L}^2 C_{i1}\alpha\right.$$

$$\left. + \frac{V}{L}\left(C_{i2}\dot{\alpha} + C_{i3}\dot{\theta}\right)\right]$$

where it is assumed that the vehicle is flying vertically and experiences only small angular deviations from the vertical path, and we define

$$\tilde{\theta} = \theta - \frac{\pi}{2}$$

so

$$\sin\theta = \cos\tilde{\theta} \cong 1$$

$$\cos\theta = \sin\tilde{\theta} \cong \tilde{\theta}$$

Some additional equations are necessary to completely describe the system. First, an expression for the control system and engine response to control-system command. Since we have assumed that the engine responds instantaneously the engine gimbal deflection angle can be set equal to the desired control command. For this study a simplified control system is considered. The thrust vector is deflected through an angle defined by the relation

$$\delta = K_1\theta + K_2\dot{\theta} + K_3(\alpha + \alpha_w)$$

K_1, K_2, and K_3 are gain constants which are selected to give a prescribed value of frequency and damping in the rigid body pitch mode at maximum dynamic pressure. The value of rigid-body uncoupled pitch mode frequency and damping chosen were $\omega_p^2 = 10(\text{rad./sec})^2$ and $\xi_p\omega_p = 2$ sec.

Two control systems are investigated. When $K_1 = 0$, the vehicle is essentially aerodynamically stable and will be referred to as α-controlled. When $K_3 = 0$, the vehicle will be referred to as θ-controlled.

The aerodynamic forces which act on the vehicle are functions of the angle of attack, that is, the angle between the velocity vector of the vehicle and the body axis. This is in still air. However, if the air is moving relative to fixed space, then the air's motion produces an additional angle of attack, which we will denote by α_w. Assume that both the still-air angle of attack, α, and the wind-induced angle of attack, α_w, are small and may be added to determine the vehicle's total angle of attack, α'.

Note that in the coordinate system used, a positive angle of attack produces a negative lift force.

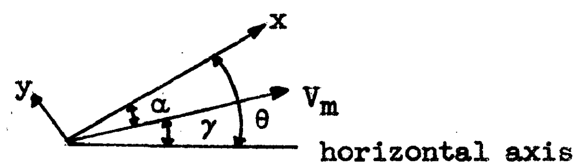

Let $V_m = \dot{x}_o^2 + \dot{y}_o^2$ = missile velocity in inertial space

V_w = horizontal wind velocity

V = velocity of moving air relative to missile

The still-air angle of attack is

$$\alpha = \theta - \gamma = \tan^{-1} \frac{-\dot{y}_o}{\dot{x}_o} = \tan^{-1} \frac{-\dot{\bar{y}}_o}{\dot{\bar{x}}_o}$$

In moving air, the angle of attack is found in the following manner

$$V^2 = V_w^2 + V_m^2 - 2V_mV_w \cos(\pi - \gamma)$$

$$= V_w^2 + V_m^2 + 2V_mV_w \cos\gamma$$

$$\doteq V_w^2 + V_m^2 - 2V_mV_w \bar{\gamma} \qquad \text{for } \bar{\gamma} = \gamma - \frac{\pi}{2} \text{ and } \bar{\gamma} \text{ small.}$$

$$\frac{V_w}{\sin \alpha_w} = \frac{V}{\sin(\pi - \gamma)}$$

$$\sin \alpha = \frac{V_w}{V} \sin(\pi - \gamma) = \frac{V_w}{V} \sin \gamma$$

$$\alpha_w = \sin^{-1} \frac{V_w}{V} \sin \gamma = \sin^{-1}\left[\frac{V_w}{V} \cos \bar{\gamma}\right]$$

Again, assuming small angles

$$\alpha \cong - \frac{\dot{y}_o}{\dot{x}_o}$$

$$\alpha_w \cong \frac{V_w}{V}$$

It is also necessary to determine the altitude in order to compute the aerodynamic forces. This is obtained from the expression

$$h = h_o + \int_o^t V_m \, d\tau$$

Finally, an expression for the bending moment is necessary. This expression is derived in appendix D and is presented there.

Solution of Equations

The solutions of linear differential equations with constant coefficients are relatively easy to obtain by known analytical methods[4,5]. Linear differential equations with coefficients which are functions of the independent variable are usually treated as a separate class, and often, are as difficult to solve as nonlinear differential equations.

However, the principle of superposition does apply to variable-coefficient linear differential equations. In the case of systems which cannot be represented by linear differential equations, direct mathematical analysis is most often impossible. It is sometimes possible to make certain assumptions to linearize these equations, to obtain valid, if restricted, results. In addition, numerical computational methods may be employed to arrive at the results.

For all classes of differential equations, however, when the forcing functions for the equations are arbitrary, and when a great many solutions are necessary, the work can be so time consuming and laborous that a complete investigation is prohibitive.

The equations of concern in this study were seen to be nonlinear variable-coefficient differential equations (although it is the author's opinion that the nonlinearity is negligible. (See chapter III.)) For some of the investigations, the equations become linear constant-coefficient equations by considering the vehicle at a discrete point in its trajectory. The scope of the investigation made it imperative to use some other means than direct mathematical analysis to obtain the desired solutions. Therefore, the results were obtained by employing a general purpose analog computer.

The general purpose analog computer is a device which obtains solutions by establishing a mathematical model of the system being considered. Components which are capable of performing integration, summation, multiplication by a constant, multiplication of two variables and a variety of other mathematical operations, are interconnected in a particular manner so as to arrive at the appropriate mathematical model. The computer represents the physical variables of the problem by electrical voltages which obey relationships similar to those obeyed by the variables themselves. The solution of nonlinear differential equations or variable-coefficient differential equations are not appreciably more difficult to obtain on an analog computer than are the solutions to linear constant-coefficient differential equations.

The process of translating the original system equations into a computer configuration which gives accurate results is called "programing". Programing techniques as well as computer operation are discussed in detail in many books[6,7].

The verification of computer results is, of course, a necessity. The computer operator must make many checks to make certain that all computer components are operating correctly and that they are interconnected so as to obey the appropriate mathematical relationships. A high degree of confidence is attained when the computer results can be checked against an independent solution of the problem. This independent solution may be obtained by mathematical methods, if possible, or on another computer. For this study an independent solution for a particular case was obtained on a high-speed digital computer. Some typical results for both the analog and digital solutions are shown in figure 12. Excellent agreement of the two solutions is apparent.

REFERENCES FOR CHAPTER I

[2]Thomson, William T. Lagrange's Equations For Moving Coordinates. STL Report No. EM 9-15, July 1959.

[3]Bisplinghoff, Raymond L., Ashley, Holt, Halfman, Robert L. Aeroelasticity. Cambridge, Mass.: Addison-Wesley Publishing Co., Inc., 1955.

[4]Ince, E. L. Ordinary Differential Equations. Dover Publications, Inc.

[5]Rainville, Earl D. Elementary Differential Equations. New York. The MacMillan Co. 1952.

[6]Johnson, Clarence L. Analog Computer Techniques. McGraw-Hill Book Co., Inc., 1956.

[7]Karplus, Walter J., and Soroka, Walter W. Analog Methods. McGraw-Hill Book Co., Inc., 1959.

CHAPTER II

RESULTS AND DISCUSSION[8]

Response to Wind Shear Reversals

The first objective to this paper was to attempt to determine significant effects resulting from using variable coefficient differential equations in a wind loads analysis of an elastic rocket. This was done, first, with the variable coefficient equations using a wind input which was a function of altitude, and second, using fixed coefficients with the wind input as a function of time. The input winds, parameter ranges covered, and pertinent results are discussed in the following sections.

Description of wind shear reversals.- The wind shear reversals which produce the loads on the rocket are triangular waves, illustrated by this sketch:

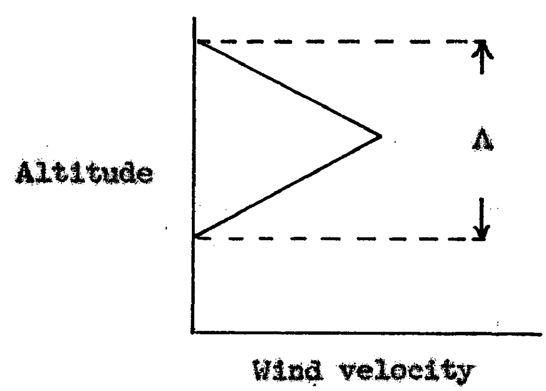

The wave is symmetric, peaking at 35,000 feet altitude near the point of maximum dynamic pressure in each trajectory. The wave length, Λ, is the total vertical distance over which the wind velocity persists.

For the variable coefficient cases, the wave is symmetric about 35,000 feet altitude. When constant coefficient cases are examined, the coefficients of the differential equations are fixed at their values at 35,000 feet, while this wind becomes a function of time rather than altitude. The time required to pass through the shear reversal, or the period, is now determined by dividing the wave length by the fixed velocity of the rocket. The maximum wind velocity occurs at one-half the period.

Bending-moment distribution.- A bending-moment distribution along the body of the vehicle is shown in figure 2 for the two basic types of control. The loads in this case resulted from a wind shear reversal of 10,000-foot wave length. In other words, the wind velocity increased linearly from zero at 30,000 feet altitude to 100 ft/sec at 35,000 feet, and then decreased linearly to zero at 40,000 feet. The maximum bending moments were determined for each type of control as the rocket ascended through this wind profile. The α-control, i.e., the control system which seeks zero angle of attack, is seen to produce larger loadings than the θ-control which maintains a constant attitude angle. The large loads when the vehicle is operated in the α-control mode result directly from large inertia loads induced by the motor. The system has no lag in the motor equation, permitting the thrust vector to follow the wind inputs, with their discontinuities, exactly as commanded by the control function. This produces large angular accelerations as well as significant excitation of the elastic modes. On the other hand, operation in the θ-control mode produces negligible inertia loads, since the thrust is vectored just enough to cancel the destabilizing aerodynamic moment, and does not excite the elastic modes to any great extent. This will be illustrated later in the paper. Also, the momentum theory aerodynamics predict very low normal forces and pitching moments on a body of revolution, such that the bending moments remain low despite the large angles of attack permitted by the θ-control system.

The maximum bending moments for these cases occur at the 0.3 and 0.5 body stations. For the remainder of the paper, the bending moment at one of these two stations is arbitrarily chosen for examination.

Bending-moment variation with frequency ratio.- Figure 3 illustrates a case where the use of variable coefficients can cause a difference in predicted loads on the rocket. The maximum bending moment at station $x = 0.5$ is shown as a function of the ratio of first bending frequency to rigid-body pitch frequency. Note that the frequency ratio, ω_1/ω_p, is a measure of the stiffness of the structure since ω_p, the rigid-body pitch frequency, has been kept constant throughout the study. The input is a 10,000-foot wave-length shear reversal with a maximum velocity of 80 ft/sec. With θ-control, the bending moments calculated using fixed coefficients are about 20 percent higher than those calculated with variable coefficients. Neither shows appreciable variation with frequency ratio, indicating small response in the elastic modes. However, the α-control behaves quite differently. The elastic modes are now contributing a large percentage of the total bending moment, causing a variation with stiffness. There is also an effect from using the variable coefficients, changing from a reduction in predicted load at low stiffness levels to an increase at higher stiffnesses. The magnitude of the predicted loads differs by over 30 percent in some ranges.

Consideration of the effects illustrated in this figure will show that they arise from the nature of the input wind. To fix the coefficients of the equations of motion, the wind becomes a function of time rather than altitude, while the rocket flies through this wind at constant velocity. In the variable coefficient case, the rocket is traveling slower at lower altitudes, and thus takes a longer time to reach the point of maximum wind. So, the transients associated with the reversal of the wind shear will occur with different phasings with respect to the previously induced motions of the vehicle. Then, depending on this phasing, which in turn will depend on the speed with which the rocket is traveling, the wave length of the shear reversal, and the frequencies of the elastic modes, the loads predicted using fixed or variable coefficients can certainly differ.

Bending-moment variation with wave length.- The differences illustrated were those due to frequency changes of the bending modes. It is anticipated that differences would also occur due to changing the wave length of the input. These are illustrated in figure 4, where bending moment is plotted against wave length of the shear reversal for two frequency ratios using angle-of-attack control. The use of fixed coefficients predicted larger loads than obtained using variable coefficients at the longer wave lengths, for the frequency ratios illustrated. However, at wave lengths below about 6,000 feet, again no difference was detectable. This is certainly in agreement with expectations for such a system - at short wave lengths, the maximum responses occur within a very short time span such that changes within the system (variable coefficients) do not have a chance to alter responses. Similar results were obtained with the attitude-control system.

Bending-moment variation with thrust-to-weight ratio.- The differences in predicted bending moments, with and without variable coefficients, which may be anticipated at different thrust-to-weight ratios are illustrated in figure 5. Bending moments at two frequency ratios are shown for the vehicle flying through a shear reversal of 10,000-foot wave length. The deviation in bending moment is largest at low T/W_o, reaching almost 20 percent, but becomes insignificant at the high values. At the high thrust-to-weight ratios, the rocket passes through the shear reversal too rapidly for the change in system parameters to effect response. The deviation in predicted bending moment appears to be about the same percent of the total for both frequency ratios at thrust-to-weight ratio 1.5.

Response to Measured Wind Profiles

The response of the elastic time varying model to measured atmospheric wind data will now be examined. All of the wind profile data which have been available to designers until recently were obtained by tracking sounding balloons. Such data are recognized to omit the small-scale fluctuations, i.e., gusts or turbulence, from the picture they present of atmospheric motion. Recently, a technique has been developed at Langley Research Center which permits these small perturbations of the wind to be measured along with the wind's gross motion. This portion of the paper will present loads for the rocket flying through one of these detailed profiles and compare them with loads produced by flying through profiles measured by conventional techniques.

Measured wind profiles.- The wind profiles are taken from reference 9 and are presented in figure 6. The detailed profile, identified as the rocket smoke trail, was determined at 100-foot altitude increments by photographic triangulation methods utilizing the exhaust trail of the rocket. Two balloon profiles are indicated - number 1 being from a balloon released 3 hours before the rocket was launched, while number 2 came from a balloon released three-quarters of an hour after rocket launch. The balloon data are seen to define the wind velocity with points about 2,000 feet apart, contrasted to the 100-foot increments in the smoke-trail data. These profiles actually extend from near sea level to over 40,000 feet altitude, but, due to limitations in the computer program, the cases reported herein cover the 20,000-to 40,000-foot altitude range.

Such mild winds would not be suitable for design purposes, but will serve for the comparisons which it is desired to make. To make the loads from the balloon data more severe, a third balloon profile, number 3, was artificially created from profile number 2 by extending one point, at 32,500 feet, until the wind velocity matched the maximum wind velocity on the smoke-trail profile. This effectively adds a wind shear reversal, with a wave length of about 4,500 feet and maximum velocity of 40 ft/sec to the existing balloon profile.

<u>Bending-moment time histories with α- and θ-control</u>.- Before comparing the responses due to the various input winds, it is convenient to examine the differences in these responses from the two types of control. Figure 7 illustrates these differences. The input wind is the balloon profile number 3 which was just described. The time history of engine gimbal angle is shown for the α-control case, along with the bending-moment response at station 0.3. The other response trace illustrated is the bending moment at station 0.3 for θ-control. With α-control, the bending moment follows the engine angle very closely. The predominant characteristics of this load are the large transient peaks, corresponding to peaks in engine angle, which occur in the regions of rapid changes in the wind input. The main component of the load would seem to be inertial, resulting from the angular accelerations of the vehicle as it follows the motor. The loads with θ-control do not exhibit this type behavior, but follow the input wind directly. With this type control, rocket attitude is being controlled which prevents large angular accelerations from occurring and large and sudden engine deflections are not required. The angle of attack follows the wind profile so that the bending moment is primarily due to aerodynamic loads. Also, since the α-control results in large, rapid engine motions, the elastic modes are responding with greater magnitude than with θ-control.

Bending-moment time histories when flying through smoke-trail wind profile.- Examples of bending-moment responses to the smoke-trail wind profile are illustrated in figure 8. In figure 8(a), the bending moment at missile station 0.3 is shown for the two types of control being considered - α-control and θ-control. The rocket parameters are $\omega_1/\omega_p = 7$ and $T/W_o = 5$. The wind profile, shown at the top as a function of time, begins at 20,000 feet altitude and ends at about 41,000 feet. Maximum dynamic pressure for this trajectory occurs at 35,000 feet, near the peak wind velocity. However, this is not necessarily the point of maximum load, as the responses show. With α-control, equal loads are produced at about 25,000 feet altitude, corresponding to the first peak on the wind profile. With θ-control the maximum bending moment does occur near the maximum wind velocity. Again, notice the difference in the form of the response of the two types of control. The α-control seeks to reduce angle of attack to zero, and, in following the wind, produces large rigid-body inertia loads as well as considerable excitation of the first and second elastic modes. On the other hand, the θ-control maintains constant attitude so that rigid-body inertia loads remain low but aerodynamic loads, due to the angle of attack induced by the wind, now become large. (Dynamic pressure for the case illustrated is approximately 5,000 lb per sq ft, so loads become large despite the small angles involved.) The net result is to produce approximately equal maximum moments at this station for both types of control.

Figure 8(b) shows the bending-moment response to the smoke-trail wind profile for three rockets of different thrust-to-weight ratios. In each case, α-control was used along with a very low stiffness - a first mode frequency only three times the rigid-body pitch frequency. Changing the thrust-to-weight ratio of the rocket changes the speed with which it traverses the wind profile and alters the dynamic pressure which the vehicle sees. It is notable, then, that the maximum loads are not too different. This comes about because, for the low thrust-to-weight ratio cases, the control system is able to keep the net angle of attack near zero, but induces large elastic responses in the process. For the $T/W_o = 5$ case, the control system is not able to reduce the net angle of attack to zero, but the elastic response is much reduced. The elastic response is the most noticeable difference between the various cases. This is to be expected since the effective frequency content of the wind changes, due to different rocket speeds, while the frequency spectrum of the structure has been held constant.

Bending-moment time histories for different wind profiles.- The differences in loads experienced by the rocket with α-control when flying through different wind profiles are illustrated in figure 9. The bending-moment response of a rocket with thrust-to-weight ratio 3 and frequency ratio 7 is shown at station 0.3 for two winds. The bending-moment time history at the top of the figure is due to the smoke-trail profile, while the bending moment shown in the bottom portion is due to the balloon profile which has been called number 3. This is the balloon-measured wind which has been adjusted by adding a shear reversal near 35,000 feet to bring the peak velocity up to that measured by the smoke-trail technique. Again, note the differences in the bending-moment response. Response to the smoke-trail profile is characterized by large first-mode contributions, while the response to the balloon profile shows larger inertia loads with greatly reduced elastic response.

<u>Maximum bending-moment variation with frequency ratio</u>.- The maximum bending moments resulting from the various wind profiles are shown in figure 10 for the rocket with thrust-to-weight ratio 5. The bending moment at station 0.5 is plotted as a function of frequency ratio for θ-control in figure 10(a), and for α-control in figure 10(b). With attitude control, the loads exhibit little variation with frequency ratio, due to slight excitation of the elastic modes. Slightly larger loads do occur at lower stiffness, as would be expected. The magnitude of the loads from the various profiles seems to correlate with the maximum wind velocities of that profile. For example, balloon profile number 2 has the lowest loads and also had the lowest wind velocities. The largest wind velocities from the balloon-measured winds were on profile number 3, seem to produce the largest loads of the three balloon profiles. However, the smoke-trail produced loads exceed those produced by balloon number 3 by 8 to 12 percent, although their maximum velocities were the same. Flying through the wind from the smoke-trail measurement produces the largest loads due to greater excitation of the elastic modes.

The picture is slightly different with α-control, figure 10(b). Now, since angle of attack is being controlled, inertia loads predominate. The balloon profile producing the largest loads is number 1, rather than number 3, due to the large transient inertia loads induced by it. In fact, the smoke-trail wind produces larger loads only at very low stiffnesses where large responses of the bending modes occur. In general, for this simple system, it would seem that bending moments are more sensitive to frequency ratio when α-control is used.

Maximum bending-moment variation with thrust-to-weight ratio.- The results just examined applied to a rocket with lift-off thrust-to-weight ratio 5.0. The loads are also influenced by this parameter, as shown in figure 11, where the maximum bending moment is plotted against thrust-to-weight ratio for two frequency ratios, $\omega_1/\omega_p = 3$ and 7, and two inputs - the smoke-trail wind profile and balloon profile number 3. The bending moment at station 0.5, with θ-control, is presented in figure 11(a), and with α-control, in figure 11(b). With attitude control, the loads increase almost linearly with thrust-to-weight ratio for both frequency ratios. Again, this is because the load is almost entirely aerodynamic resulting from the angle of attack built up by the wind. The bending moments due to the smoke-trail wind are greater than those due to flying the balloon-measured profile in every case, ranging up to almost 15 percent at the higher thrust-to-weight ratios. And again, it should be noted that the lower stiffness produced higher loads, for both inputs, over the entire range of thrust weight ratios investigated.

The observations that lower stiffnesses and the smoke-trail input produce higher bending moments carry over to the α-control case, figure 11(b). But now the trend with thrust-to-weight ratio is reversed. Where, with θ-control, loads increased with this ratio, they decrease when using α-control. This is explained by recalling that, with α-control, loads are primarily inertial, produced by engine deflections as the rocket tries to keep angle of attack zero. At high thrust-to-weight ratios, rocket velocity is higher so that effective angle of attack due to the wind is reduced. Thus, less control is required to keep the net angle of attack zero and loads go down. Also, with this type control, where bending response produces a larger portion of the load, the differences between the loads produced by the two wind profiles are seen to vary much more with frequency ratio. The low stiffness, $\omega_1/\omega_p = 3$, shows a very large increase in load, while the frequency ratio 7 case shows only moderate increases.

REFERENCES FOR CHAPTER II

[8] Morgan, H. G., and Baron, S. Wind Loads On a Vertically Rising Vehicle Including Effects of Time-Varying Coefficients. Presented to the Symposium on Structural Dynamics of High-Speed Flight. Los Angeles, Calif., April 1961.

[9] Henry, Robert M., Brandon, George W., Tolefson, Harold B., and Lanford, Wade E. A Method for Obtaining Detailed Wind Shear Measurements for Application to Dynamic Response Problems of Missile Systems. NASA Langley Research Center. Proposed TN.

CHAPTER III

FUTURE CONSIDERATIONS

Some further investigation with this simple model seems to be indicated. However, it is the author's feeling that the present system can be simplified still further so as to ease the analysis.

The most important simplification would be to linearize the system. First we note that for most considerations we may set $V = \dot{x}_o$. Then, if we consider the equations we see that the only nonlinear term is the centrifugal force term appearing in the $\ddot{x}_o$ equation, for if this term were neglected, then $\dot{x}_o$ would be simply a function of time given by

$$\dot{x}_o = -\frac{g}{L} t + \frac{g}{L} I_{sp} \ln \left[\frac{1}{1 - \frac{T/W_o}{I_{sp}} t} \right]$$

The equations would then be linear differential equations with time-varying coefficients. Examining this term and noting that $\dot{\theta}$ is a controlled quantity and for the winds that are being considered $\dot{y}_o$ would tend to be small, it seems likely that the product would indeed be small compared to the component of force produced by the thrust.

Instead of just omitting this term from the equation, it was decided, instead, to examine the complete set of equations to see if superposition holds. If it does then the system may be considered linear. Several such linearity checks were made and a typical one is shown in figure 13.

A further simplification which might be made in this case is to consider only the first elastic mode, neglecting all others. This simplification was indicated on the basis of the runs made in this study. It was observed that the second mode contribution to the bending-moment response was extremely small and the third mode undetectable. This can be explained in terms of the wide separation of natural frequencies of the normal modes for a uniform beam. A similar assumption for a realistic vehicle would be much less in order.

With these simplifications the system reduces to three degrees of freedom, two rigid body modes and one elastic mode. The equations are linear time-varying differential equations.

One of the chief advantages in having a linear system is that the response to random disturbances is more easily studied. If the input to a linear system is a normally distributed random process then the response is normally distributed. Thus it is only necessary to compute the average and the covariance in order to define the probability distribution of the response[10]. An examination of the wind data available indicates that the atmosphere is a nonstationary random process. A study of the bending-moment response for a rigid vehicle to nonstationary random inputs using a high-speed digital computer is described in reference 10. The author feels that the application of the analog computer to the same problem, with the inclusion of elastic effects, is an area for further investigation.

Further, the application of specific analog computation techniques may prove fruitful. One such technique is the "Adjoint Method"[11], a method which reduces the labor involved in studying the response of linear time-varying systems. The adjoint method yields in a single computer run a weighting function, which by conventional methods requires a large, if not infinite, number of runs[12]. The response to a large variety of inputs, including arbitrary inputs can be determined in one computer run. Particularly, the mean square response to white Gaussian noise is readily attainable. The possible extension of this technique to nonstationary random process is an area for future study.

The present study included the variation of bending-moment response with thrust-to-weight ratio and frequency ratio. Several other parameters influence the response, e.g., length of vehicle, specific impulse. The effects of these other parameters on the bending-moment response should be determined. In connection with the study of the effects of various parameters the possible use of "parameter influence coefficients"[13] will be considered.

REFERENCES FOR CHAPTER III

[10] Beiber, R. E. Missile Structural Loads by Non-Stationary Statistical Methods. Journal of Aerospace Sciences, vol. 28, no. 4, April 1961, pp. 284-294.

[11] Laning, J. Halcombe, and Batten, Richard H. Random Processes in Automatic Control. McGraw-Hill Book Company, Inc., 1956.

[12] Fifer, Stanley. Analog Computation. Vol. IV. McGraw-Hill Book Co., Inc., 1961.

[13] Meissinger, Hans F. The Use of Parameter Influence Coefficients in Computer Analysis of Dynamic Systems.

APPENDIX A

AERODYNAMIC FORCES

The aerodynamic forces acting on the missile will be computed using slender body theory as described in reference 14. Following the reference, the lift distribution along the axis of the body is given by

$$l(\bar{x},t) = -\rho\left(\frac{V}{L}\frac{\partial}{\partial\bar{x}} - \frac{\partial}{\partial t}\right)S(\bar{x})W(\bar{x},t)$$

where $S(\bar{x})$ is the cross-sectional area distribution along the center line of the missile and $W(\bar{x},t)$ is the downwash velocity of the fluid. As suggested by the reference, and for simplicity, the contributions of the elastic motions to the downwash will be neglected, and the downwash will be given by

$$W(\bar{x},t) = V\alpha' - L(\bar{x} - \bar{x}_{c.g.})\dot{\theta}$$

Thus, the lift distribution becomes

$$l(\bar{x},t) = -\rho V\left\{S'(\bar{x})\left[\frac{V}{L}\alpha' - (\bar{x} - \bar{x}_{c.g.})\dot{\theta}\right] + S(\bar{x})\left[-\dot{\theta}\right]\right\} + \rho S(\bar{x})\, V\dot{\alpha}$$

where, for simplicity, it is assumed $\alpha' = \dot{\alpha}$. Aerodynamic forces and moments acting on the missile are found by integrating this lift distribution as follows:

$$F_{yA} = L \int_0^1 l(\bar{x},t)d\bar{x}$$

$$M_{zA} = L^2 \int_0^1 (\bar{x} - \bar{x}_{c.g.})l(\bar{x},t)d\bar{x}$$

$$Q_{iA} = L \int_0^1 \varphi_i(\bar{x})l(\bar{x},t)d\bar{x}$$

Performing the indicated operations, we get for these forces and moments

$$F_{yA} = \rho S_o \left\{ V^2\alpha' + V\left[\bar{x}_{c.g.}\dot{\theta} + \left(L \int_0^1 \frac{S(\bar{x})}{S_o}\, d\bar{x}\right)\dot{\alpha}\right]\right\}$$

$$M_{zA} = \rho S_o \left\{ V^2\left[L \int_0^1 \frac{S(\bar{x})}{S_o}\, d\bar{x}\right]\alpha' - V\left[L^2 \int_0^1 (\bar{x} - \bar{x}_{c.g.}) \frac{S(\bar{x})}{S_o}\, d\bar{x}\right]\dot{\theta} \right.$$
$$\left. + V\left[L^2 \int_0^1 \bar{x}\, \frac{S(\bar{x})}{S_o}\, d\bar{x}\right]\dot{\alpha}\right\} - \bar{x}_{c.g.}LF_{yA}$$

$$Q_{iA} = \rho S_o \left\{ -V^2 \left[\int_0^1 \varphi_i(\bar{x}) \frac{S'(\bar{x})}{S_o}\, d\bar{x}\right]\alpha' + V\left[L \int_0^1 (\bar{x} - \bar{x}_{c.g.})\varphi_i(\bar{x}) \frac{S'(\bar{x})}{S_o} \right.\right.$$
$$\left.\left. + \varphi_i(\bar{x}) \frac{S(\bar{x})}{S_o}\, d\bar{x}\right]\dot{\theta} + V\left[L \int_0^1 \varphi_i(\bar{x}) \frac{S(\bar{x})}{S_o}\, d\bar{x}\right]\dot{\alpha}\right\}$$

Nondimensionalizing these equations, we get for the aerodynamic forces

$$\frac{F_{yA}}{ML} = \frac{\rho_o S_o L}{M_o}\,\frac{\rho}{\rho_o}\,\frac{M_o}{M}\left\{\left(\frac{V}{L}\right)^2\alpha' + \frac{V}{L}\left[\bar{x}_{c.g.}\dot{\theta} + \left(\int_o^1 \frac{S(\bar{x})}{S_o}\,d\bar{x}\right)\dot{\alpha}\right]\right\}$$

$$\frac{M_{zA}}{ML^2} = \frac{\rho_o S_o L}{M_o}\,\frac{\rho}{\rho_o}\,\frac{M_o}{M}\left\{\left(\frac{V}{L}\right)^2\left[\int_o^1 \frac{S(\bar{x})}{S_o}\,d\bar{x}\right]\alpha' - \frac{V}{L}\left[\int_o^1 (\bar{x} - \bar{x}_{c.g.})\,\frac{S(\bar{x})}{S_o}\,dx\right]\dot{\theta}\right.$$

$$\left. + \frac{V}{L}\left[\int_o^1 \bar{x}\,\frac{S(\bar{x})}{S_o}\,d\bar{x}\right]\dot{\alpha}\right\} - \bar{x}_{c.g.}\,\frac{F_{yA}}{ML}$$

$$\frac{Q_{iA}}{Ml} = \frac{\rho_o S_o L}{M_o}\,\frac{\rho}{\rho_o}\,\frac{M_o}{M}\left\{-\left(\frac{V}{L}\right)^2\left[\int_o^1 \varphi_i(\bar{x})\,\frac{S'(\bar{x})}{S_o}\,d\bar{x}\right]\alpha'\right.$$

$$+ \frac{V}{L}\left[\int_o^1 (\bar{x} - \bar{x}_{c.g.})\left(\varphi_i(\bar{x})\,\frac{S'(\bar{x})}{S_o}\right) + \varphi_i(\bar{x})\,\frac{S(\bar{x})}{S_o}\,d\bar{x}\right]\dot{\theta}$$

$$\left. + \frac{V}{L}\left[\int_o^1 \varphi_i(\bar{x})\,\frac{S(\bar{x})}{S_o}\,d\bar{x}\right]\dot{\alpha}\right\}$$

Or, for the aerodynamics in the elastic equations

$$\frac{Q_{iA}}{ML} = \frac{\rho_o S_o L}{M_o}\,\frac{\rho}{\rho_o}\,\frac{M_o}{M}\left\{\left(\frac{V}{L}\right)^2 C_{i1}\alpha' + \frac{V}{L}\left(C_{i2}\dot{\alpha} + C_{i3}\dot{\theta}\right)\right\}$$

where

$$C_{i1} = -\int_o^1 \varphi_i(\bar{x})\,\frac{S'(\bar{x})}{S_o}\,d\bar{x}$$

$$C_{i2} = \int_o^1 \varphi_i(\bar{x})\,\frac{S(\bar{x})}{S_o}\,d\bar{x}$$

$$C_{i3} = \int_o^1 \bar{x}\varphi_i(\bar{x})\,\frac{S'(\bar{x})}{S_o}\,d\bar{x} + C_{i2} + \bar{x}_{c.g.}C_{i1}$$

REFERENCE FOR APPENDIX A

[14] Miles, J. W., and Young, Dana. Generalized Missile Dynamics Analysis, III - Aerodynamics. STL Report No. EM 8-9, April 1958.

APPENDIX B

JET FORCES AND MOMENTS

The method of reference 15 will be used to determine the forces and moments acting on the missile due to the rocket exhaust. From reference 15, the force acting on the missile at the face of the rocket exhaust due to outflowing gas is

$$\bar{F}_j = -\int_A \rho\bar{v}(\bar{v}_r \cdot d\bar{A})$$

and the moment about the center of gravity is

$$\bar{M}_j = -\int_A \bar{r} \times \rho\bar{v}_1(\bar{v}_r \cdot d\bar{A})$$

where the integrations are to be performed over the area A of the rocket exhaust. In these equations, ρ is the density of the exhaust gas, $\bar{v}$ is the vector velocity of the exiting fluid, $\bar{v}_1$ is the velocity of the exiting fluid relative to the c.g., $\bar{v}_r$ is the velocity of the exiting fluid relative to the exhausting surface, $d\bar{A}$ is a differential area vector in the direction of fluid outflow, and $\bar{r}$ is the vector locating the exhaust relative to the c.g.

To compute the jet forces for the present system, the vector quantities can be written as

$$d\bar{A} = -dA\left[\cos(u_e' + \delta)\,\bar{i} + \sin(u_e' + \delta)\,\bar{j}\right]$$

$$\bar{v} = \left[\dot{x}_o - v_e \cos(u_e' + \delta)\right]\bar{i} + \left[\dot{y}_o - l_e\dot{\theta} - v_e \sin(u_e' + \delta) + \dot{u}_e\right]\bar{j}$$

$$\bar{v}_r = \left[-v_e \cos(u_e' + \delta)\right]\bar{i} + \left[-v_e \sin(u_e' + \delta)\right]\bar{j}$$

$$\bar{v}_l = \left[-v_e \cos(u_e' + \delta)\right]\bar{i} + \left[-l_e\dot{\theta} - v_e \sin(u_e' + \delta) + \dot{u}_e\right]\bar{j}$$

$$\bar{r} = -l_e\,\bar{i} + u_e\,\bar{j}$$

where $\bar{i}$, $\bar{j}$, $\bar{k}$ are unit vectors along the body axes at the c.g. Performing the indicated operations, we can find the jet forces as follows:

$$\bar{v}_r \cdot dA = v_e dA$$

Now, assuming the outflow of gas is uniformly distributed over the exhausting surface of the rocket,

$$\bar{F}_j = -\rho v_e \int_A \bar{v}\,dA = -\rho v_e A\bar{v}$$

$$= -\rho v_e A\left\{\left[\dot{x}_o - v_e \cos(u_e' + \delta)\right]\bar{i} + \left[\dot{y}_o - l_e\dot{\theta} - v_e \sin(u_e' + \delta) + \dot{u}_e\right]\bar{j}\right\}$$

and

$$M_j = -\rho v_e A\bar{r} \times \bar{v}_l$$

$$= -\rho v_e A\left\{v_e u_e \cos(u_e' + \delta) + v_e l_e \sin(u_e' + \delta) + l_e^2\dot{\theta} - l_e\dot{u}_e\right\}\bar{k}$$

A pressure force, due to the back pressure on the nozzle, face, also acts on the missile. This force is normally combined with the jet force to give the thrust. If the back pressure is given by p_e, then the vector components of the force due to it are

$$\text{pressure force} = p_e A \left\{ \cos(u_e' + \delta)\,\bar{i} + \sin(u_e' + \delta)\,\bar{j} \right\}$$

and the moment produced about the c.g. is

$$\text{pressure moment} = -p_e A \left\{ l_e \sin(u_e' + \delta) + u_e \cos(u_e' + \delta) \right\} \bar{k}$$

Now, combining the jet and back pressure terms, the components of force and moment acting on the vehicle become

$$F_{x_e} = -\rho v_e A \left[\dot{x}_o - v_e \cos(u_e' + \delta) \right] + p_e A \cos(u_e' + \delta)$$

$$F_{y_e} = -\rho v_e A \left[\dot{y}_o - l_e \dot{\theta} - v_e \sin(u_e' + \delta) + \dot{u}_e \right] + p_e A \sin(u_e' + \delta)$$

$$M_{z_e} = -\rho v_e A \left[v_e u_e \cos(u_e' + \delta) + v_e l_e \sin(u_e' + \delta) + l_e^2 \dot{\theta} - l_e \dot{u}_e \right]$$

$$- p_e A \left[l_e \sin(u_e' + \delta) + u_e \cos(u_e' + \delta) \right]$$

Define the thrust as

$$T = \rho A v_e^2 + p_e A$$

and noting that the mass flow rate is given by

$$\dot{M} = -\rho A v_e$$

we get for these forces and moments

$$F_{x_e} = \dot{M} \dot{x}_o + T \cos(u_e' + \delta)$$

$$F_{y_e} = \dot{M} \left[\dot{y}_o - l_e \dot{\theta} + \dot{u}_e \right] + T \sin(u_e' + \delta)$$

$$M_{z_e} = \dot{M} \left[l_e^2 \dot{\theta} - l_e \dot{u}_e \right] - T \left[l_e \sin(u_e' + \delta) + u_e \cos(u_e' + \delta) \right]$$

If the angles δ and u_e' are assumed small such that $\cos(u_e' + \delta) \approx 1$ and $\sin(u_e' + \delta) = u_e' + \delta$, these equations are

$$F_{x_e} = \dot{M}\dot{x}_o + T$$

$$F_{y_e} = \dot{M}\left[\dot{y}_o - l_e\dot{\theta} + \dot{u}_e\right] + T(u_e' + \delta)$$

$$M_{z_e} = \dot{M}\left[l_e^2\dot{\theta} - l_e\dot{u}_e\right] - T\left[l_e(u_e' + \delta) + u_e\right]$$

or, when the elastic deformation is assumed to be made up of a summation of normal modes

$$u(x,t) = \sum_i \varphi_i(x)q_i(t)$$

$$F_{x_e} = \dot{M}\dot{x}_o + T$$

$$F_{y_e} = \dot{M}\left[\dot{y}_o - l_e\dot{\theta} + \sum_i \varphi_i(o)\dot{q}_i(t)\right] + T\left[\delta + \sum_i \varphi_i'(o)q_i(t)\right]$$

$$M_{z_e} = \dot{M}\left[l_e^2\dot{\theta} - l_e \sum_i \varphi_i(o)\dot{q}_i(t)\right] - T\left[l_e\left(\delta + \sum_i \varphi_i'(o)q_i(t)\right)\right.$$

$$\left. + \sum_i \varphi_i(o)q_i(t)\right]$$

REFERENCE FOR APPENDIX B

[15] Hausner, George W., and Hudson, Donald E. Applied Mechanics Dynamics. Van Nostrand Company, Inc., Princeton, N. J., 1950.

APPENDIX C

UNIFORM BEAM CONSTANTS

The equations of motion can be simplified by assuming the missile under consideration behaves like a uniform beam. Thus, the mode shapes are known and can be taken from any convenient reference[16].

With the mode shapes normalized to give unit deflection at the trailing edge of the missile ($\bar{x} = 0$), the constants in the equations of motion can be listed as follows

$$\varphi_i(0) = 1.0, \quad i = 1,2,3$$

$$\varphi_1'(0) = -4.647$$

$$\varphi_2'(0) = -7.859$$

$$\varphi_3'(0) = -11.0$$

$$A_i = \int_0^1 \left[\varphi_i(\bar{x})\right]^2 d\bar{x} = \frac{1}{4}, \quad i = 1,2,3$$

In addition, the following geometric constants can also be listed.

$$\frac{l_e}{L} = \frac{1}{2}$$

$$\left(\frac{k}{L}\right)^2 = \frac{1}{12}$$

$$\bar{x}_{c.g.} = \frac{1}{2}$$

REFERENCE FOR APPENDIX C

[16]Bisplinghoff, Raymond L., Ashley, Holt, Halfman, Robert L. Aeroelasticity. Cambridge, Mass.: Addison-Wesley Publishing Co., Inc., 1955.

APPENDIX D

BENDING MOMENTS

The bending moment acting at any station along the missile will be found by the modal acceleration method. That is, the loads along the missile will be found, and then the moment due to these loads computed. Loads which will be considered are aerodynamic and inertial.

The loads at any station are

Aerodynamic:

$$p_a(\bar{x},t) = l(\bar{x},t) = -\rho V \left\{ S'(\bar{x}) \left[\left(\frac{V}{L}\right)\alpha' + (\bar{x} - \bar{x}_{c.g.})\dot{\bar{\theta}} \right] + S(\bar{x}) \left[-\dot{\bar{\theta}} \right] \right\}$$

$$+ \rho S(\bar{x}) \left\{ V\dot{\alpha}' \right\}$$

Inertial:

$$p_i(x,t) = -Lm(\bar{x}) \left\{ (\ddot{\bar{y}}_o + \ddot{\bar{\theta}}\bar{x}_o - \frac{g}{L}\,\bar{\theta}) + (\bar{x} - \bar{x}_{c.g.})\ddot{\bar{\theta}} + \sum_j \varphi_j(\bar{x})\ddot{\bar{q}}_j(t) \right\}$$

Then the moment at a station $\bar{x}$ is given by

$$B.M.(x) = L^2 \int_{\bar{x}}^{1} (\bar{\xi} - \bar{x}) \left[p_a(\bar{\xi},t) + p_i(\bar{\xi},t) \right] d\bar{\xi}$$

Substituting for $p_a(\bar{x},t)$ and $p_i(\bar{x},t)$ and noting that $LM(\bar{\xi}) = M$, we may express the bending moment as

$$B.M.(\bar{x}) = L^2\left\{(\rho S_o L)\int_{\bar{x}}^{1}(\bar{\xi}-\bar{x})\left[-\left(\frac{V}{L}\right)^2\frac{S'(\bar{\xi})}{S_o}\alpha' - \left(\frac{V}{L}\right)(\bar{\xi}-\bar{\xi}_{c.g.})\frac{S'(\bar{\xi})}{S_o}\dot{\theta}\right.\right.$$

$$\left. + \left(\frac{V}{L}\right)\frac{S(\bar{\xi})}{S_o}\dot{\theta} + \left(\frac{V}{L}\right)\frac{S(\bar{\xi})}{S_o}\dot{\alpha}\right] - M\int_{\bar{x}}^{1}(\bar{\xi}-\bar{x})\left[\left(\ddot{\bar{y}}_o + \dot{\theta}\dot{\bar{x}}_o - \frac{g}{L}\bar{\theta}\right)\right.$$

$$\left.\left. + (\bar{\xi}-\bar{\xi}_{c.g.})\ddot{\theta} + \sum_j \varphi_j(\bar{\xi})\ddot{\bar{q}}_j\right]d\bar{\xi}\right\}$$

The aerodynamic integrals required are

$$\int_{\bar{x}}^{1}(\bar{\xi}-\bar{x})\frac{S'(\bar{\xi})}{S_o}d\bar{\xi} \equiv -D_1$$

$$\int_{\bar{x}}^{1}(\bar{\xi}-\bar{x})\left\{(\bar{\xi}-\bar{\xi}_{c.g.})\frac{S'(\bar{\xi})}{S_o} - \frac{S(\bar{\xi})}{S_o}\right\}d\bar{\xi} \equiv -D_2$$

$$\int_{\bar{x}}^{1}(\bar{\xi}-\bar{x})\frac{S(\bar{\xi})}{S_o}d\bar{\xi} \equiv D_3$$

Noting that $\frac{S(\bar{\xi})}{S_o} = \left[1-\bar{\xi}^2\right]^2$ and $\bar{\xi}_{c.g.} = \frac{1}{2}$ evaluating the integrals yields

$$-D_1 = -\left[\frac{8}{15} - \bar{x}\left(1 - \frac{2}{3}\bar{x}^2 + \frac{1}{5}\bar{x}^4\right)\right]$$

$$-D_2 = \left[-\frac{3}{5} + \frac{31}{30}\bar{x} - \frac{1}{3}\bar{x}^3 - \frac{1}{3}\bar{x}^4 + \frac{1}{10}\bar{x}^5 + \frac{2}{15}\bar{x}^6\right]$$

$$D_3 = \left[\frac{1}{6} - \frac{8}{15}\bar{x} + \frac{1}{2}\bar{x}^2 - \frac{1}{6}\bar{x}^4 + \frac{1}{30}\bar{x}^6\right]$$

The integrals necessary for the inertial contributions to the bending moment are

$$\int_{\bar{x}}^{1} (\bar{\xi} - \bar{x})d\bar{\xi} \equiv -D_4$$

$$\int_{\bar{x}}^{1} (\bar{\xi} - \bar{x})(\bar{\xi} - \bar{\xi}_{c.g.})d\bar{\xi} \equiv -D_5$$

$$\int_{\bar{x}}^{1} (\bar{\xi} - \bar{x})\varphi_j(\bar{\xi})d\bar{\xi} = -D_{nj}$$

Evaluating these integrals yields

$$-D_4 = \frac{1}{2}(1 - \bar{x})^2$$

$$-D_5 = \frac{1}{12}(1 + 2\bar{x})(1 - \bar{x})^2$$

$$D_{nj} = -D_4\varphi_j(\bar{\xi})$$

Algebraic manipulation then leads to the following expression for the nondimensional bending moment

$$\frac{B.M.(x)}{W_oL} = \frac{\rho_oS_oL}{M_o}\,\frac{\rho}{\rho_o}\,\frac{1}{g/L}\left\{\left(\frac{V}{L}\right)^2 D_1\alpha' + \frac{V}{L}\left(D_2\dot{\alpha} + D_3\dot{\theta}\right)\right\}$$
$$- \frac{T/W_o}{I_{sp}\,\frac{g}{L}\,\frac{\dot{M}}{M}}\left\{D_4\left[\ddot{\bar{y}}_o + \ddot{\bar{\theta}}\bar{x}_o - \frac{g}{L}\,\bar{\theta}\right] + D_5\ddot{\bar{\theta}} + \sum_j D_{nj}\ddot{\bar{q}}_j\right\}$$

The constants appearing in the equation were evaluated for the stations of interest and are listed in Table I.

BIBLIOGRAPHY

Beiber, R. E. Missile Structural Loads by Non-Stationary Statistical Methods. Journal of Aerospace Sciences. Vol. 28, No. 4, April 1961, pp. 284-294.

Bisplinghoff, Raymond L., Ashley, Holt, Halfman, Robert L. Aeroelasticity. Cambridge, Mass.: Addision-Wesley Publishing Co., Inc., 1955.

Crandall, Stephen H. Random Vibration. Technology Press of the Massachusetts Institute of Technology.

Fifer, Stanley. Analog Computation. Vol. IV, McGraw-Hill Book Co., Inc., 1961.

Geissler, Ernst D. Problems in Attitude Stabilization of Large Guided Missiles. Aerospace Engineering, Vol. 19, No. 10, October 1960, pp. 24-29, 68-72.

Hausner, George W., and Hudson, Donald E. Applied Mechanics Dynamics. Van Nostrand Company, Inc., Princeton, N.J., 1950.

Henry, Robert M., Brandon, George W., Tolefson, Harold B., and Lanford, Wade E. A Method for Obtaining Detailed Wind Shear Measurements for Application to Dynamic Response Problems of Missile Systems. NASA, Langley Research Center, Proposed TN.

Ince, E. L. Ordinary Differential Equations. Dover Publications, Inc.

Johnson, Clarence L. Analog Computer Techniques. McGraw-Hill Book Co., Inc., 1956.

Karplus, Walter J., and Soroka, Walter W. Analog Methods. McGraw-Hill Book Co., Inc., 1959.

Laning, J. Halcombe, and Batten, Richard H. Random Processes in Automatic Control. McGraw-Hill Book Company, Inc., 1956.

Meissinger, Hans F. The Use of Parameter Influence Coefficients in Computer Analysis of Dynamic Systems.

Miles, J. W., and Young, Dana. Generalized Missile Dynamics Analysis, III - Aerodynamics. STL Report No. EM 8-9, April 1958.

Morgan, H. G., and Baron, S. Wind Loads On a Vertically Rising Vehicle Including Effects of Time-Varying Coefficients. Presented to the Symposium on Structural Dynamics of High-Speed Flight, Los Angeles, Calif., April 1961.

Rainville, Earl D. Elementary Differential Equations. New York: The MacMillan Co., 1952.

Rogers, A. E., and Connolly, T. N. Analog Computation in Engineering Design. McGraw-Hill Book Co., Inc., 1960.

Thomson, William T. Lagrange's Equations For Moving Coordinates. STL Report No. EM 9-15, July 1959.

VITA

Sheldon Baron

Born in Brooklyn, N. Y. May 13, 1934. Graduated from Boys High School in that city, January 1951; B.S.; Brooklyn College, 1955.

Entered on active duty with USAF as Second Lt. August 1955. Completed active duty, August 1957. Assigned to NACA for that period.

Employed by the NASA from February 1958 to present time. Experience totals in excess of five years, in the field of programing and operating analog computer and system analysis.

TABLE II.- NUMERICAL DATA

$I_{sp} = 250$ sec

$g/L = \frac{1}{2} \frac{1}{\sec^2}$

$\frac{\rho_o S_o L}{M_o} = .0025$

$i \backslash j$	1	2	3
1	-0.223	-0.0108	-0.0169
2	0	-.0185	-.0739
3	-.0181	.00136	.00983

(Column heading: C_{ij})

x_n	D_1	D_2	D_3	D_4	D_5	D_{n1}	D_{n2}	D_{n3}
0	0.533	0.1667	0.100	-0.500	-0.0833	0	0	0
.10	.434	.118	.05528	-.405	-.0810	-.00423	-.00369	-.00326
.20	.339	.0797	.02185	-.320	-.0747	-.0138	-.00979	-.00649
.30	.251	.0503	-.00017	-.245	-.0653	-.0245	-.0122	-.00407
.35	.211	.0388	-.00718	-.211	-.0598	-.0290	-.0111	-.00114
.40	.174	.0292	-.01181	-.180	-.0540	-.0325	-.00844	.00190
.45	.140	.0214	-.01434	-.151	-.0479	-.0348	-.00459	-.00414
.50	.110	.0151	-.01510	-.125	-.0417	-.0355	0	-.00490
.55	.0842	.0103	-.01446	-.101	-.0354	-.0348	.00459	-.00414
.60	.0618	.0066	-.01280	-.080	-.0293	-.0325	.00844	-.00190
.65	.0432	.0040	-.01049	-.061	-.0235	-.0290	.0111	-.00114
.70	.0284	.0022	-.00792	-.045	-.0180	-.0245	.0122	-.00407
.80	.0091	.0005	-.00321	-.020	-.0087	-.0138	.00979	-.00649
.90	.0012	.00003	-.00053	-.005	-.0023	-.00423	.00369	-.00326
1.00	0	0	0	0	0	0	0	0

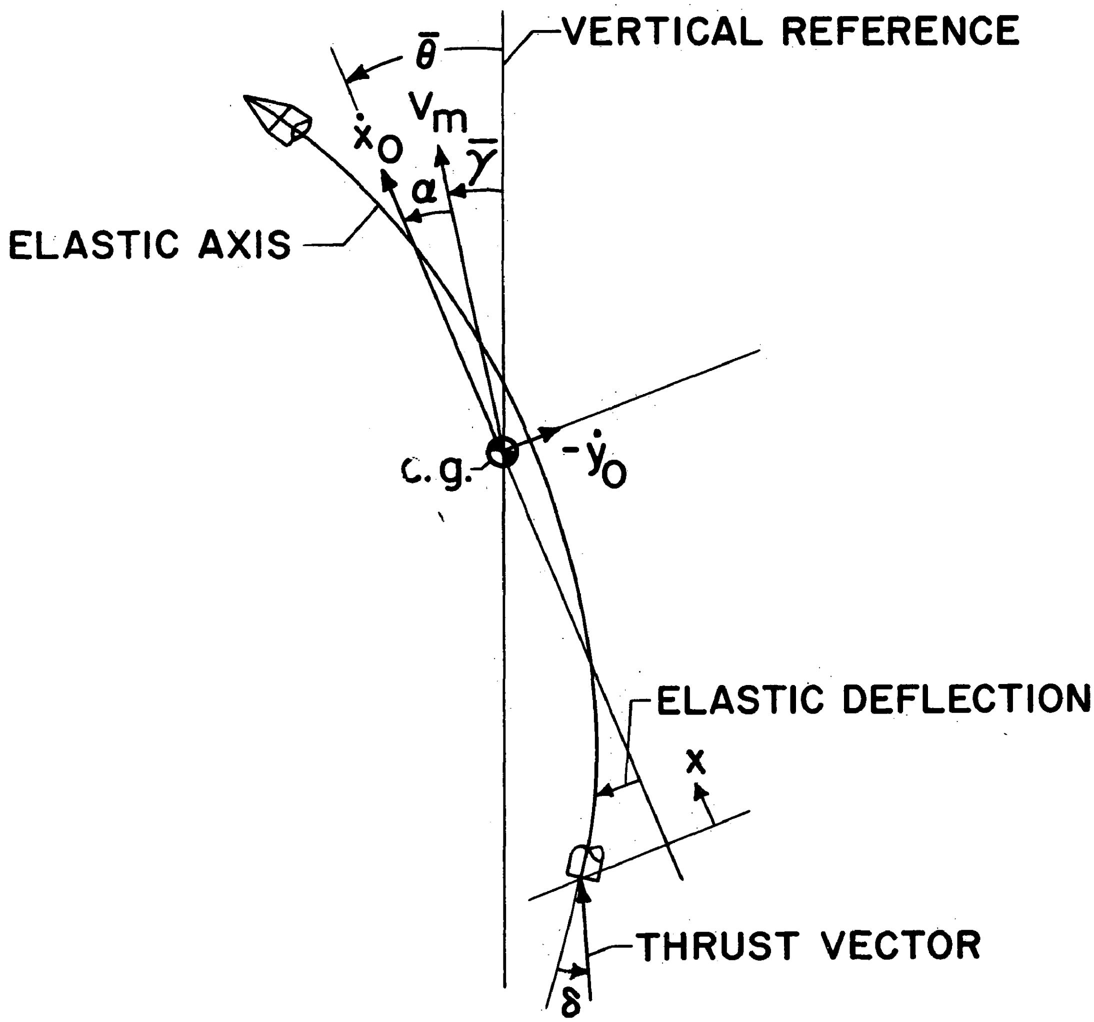

Figure 1.- Coordinate system for ascending rocket.

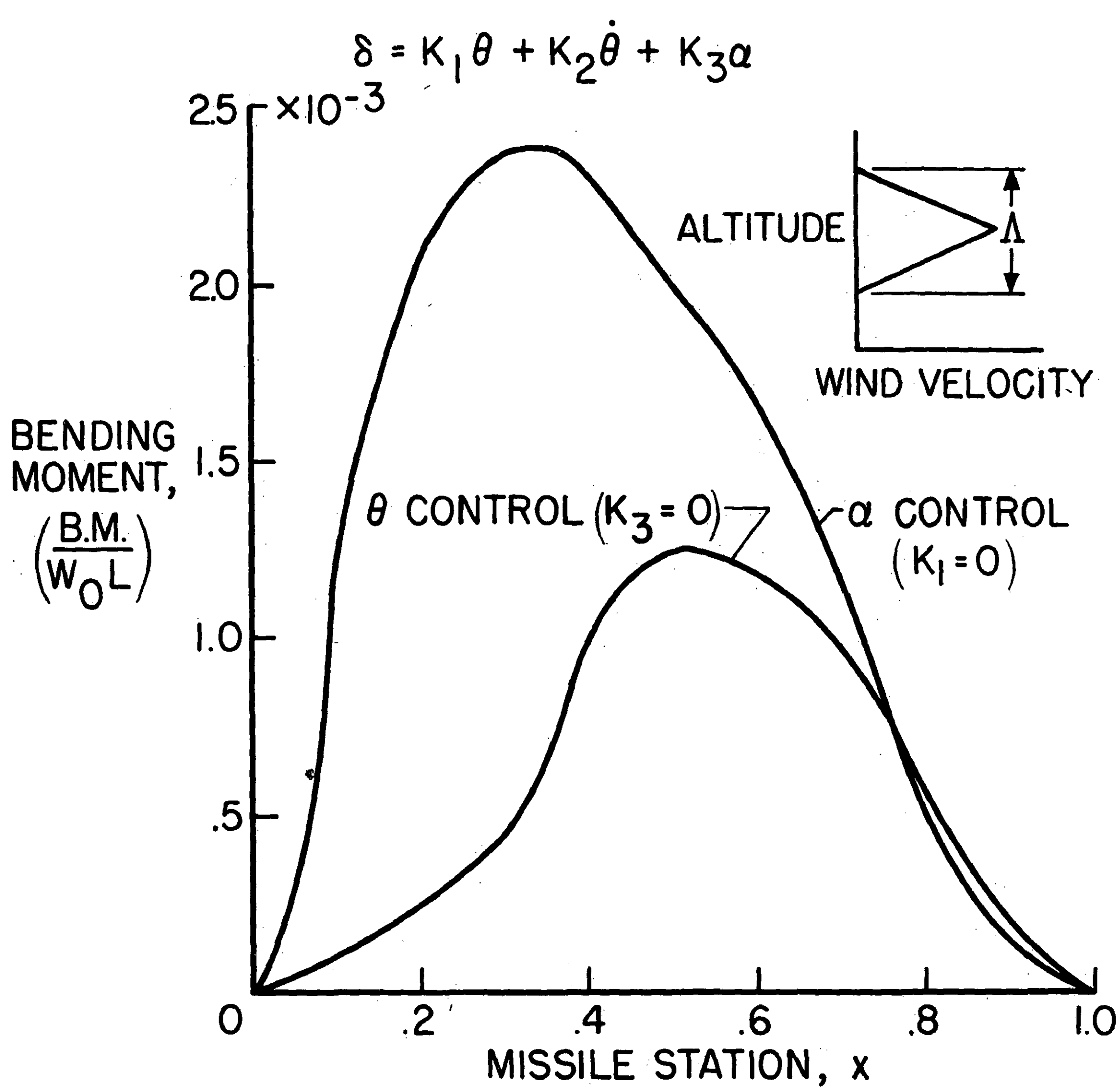

Figure 2.- Bending-moment distribution along missile. Λ = 10,000 ft, $\left(V_w\right)_{max}$ = 100 ft/sec, $\frac{\omega_1}{\omega_p}$ = 8.66.

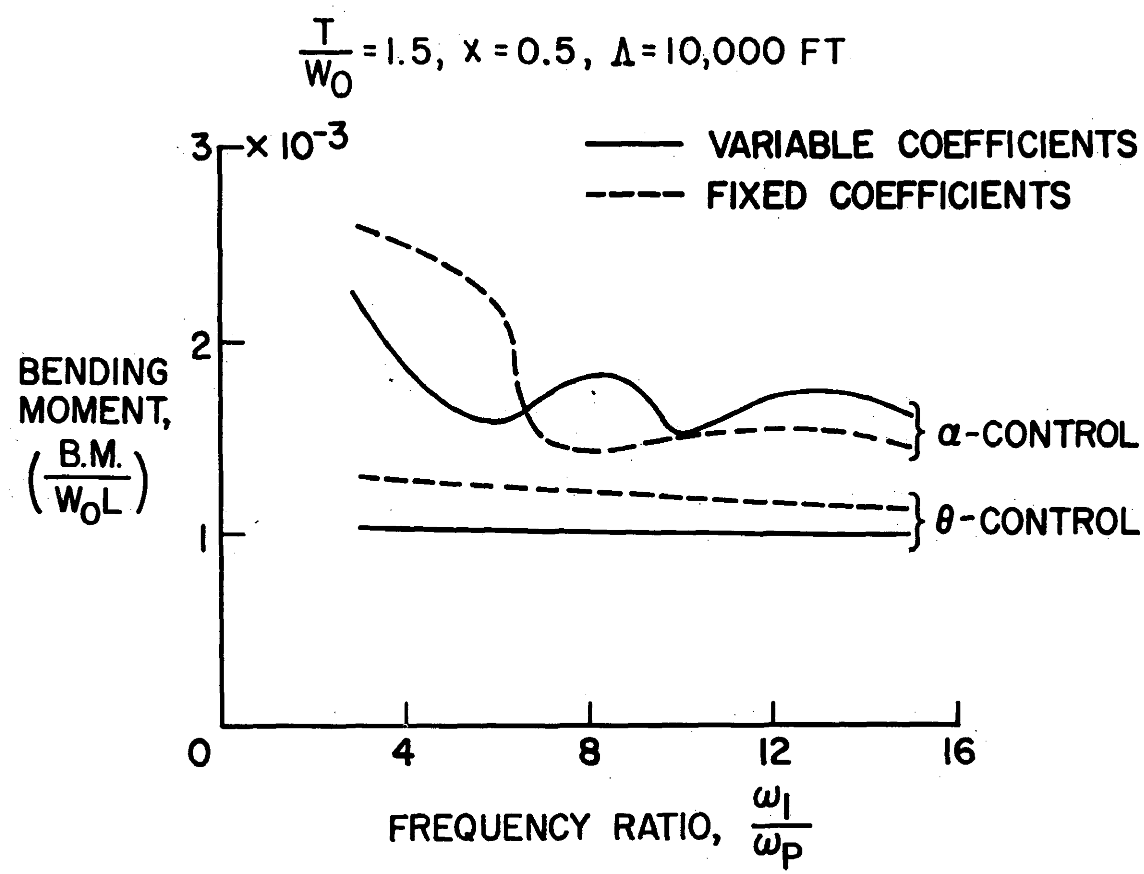

Figure 3.- Maximum bending-moment variation with frequency ratio. $(V_w)_{max} = 80$ ft/sec.

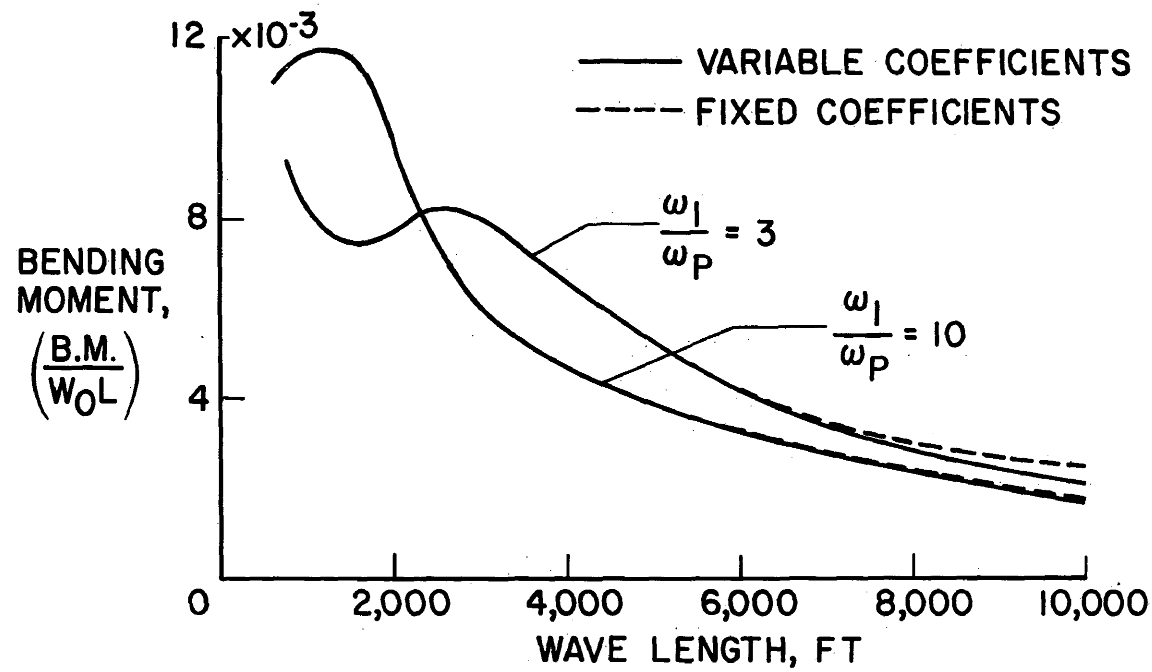

Figure 4.- Maximum bending-moment variation with wave length of shear reversal using α-control. $\frac{T}{W_o} = 1.5$, $x = 0.5$, $\left(V_w\right)_{max} = 100$ ft/sec.

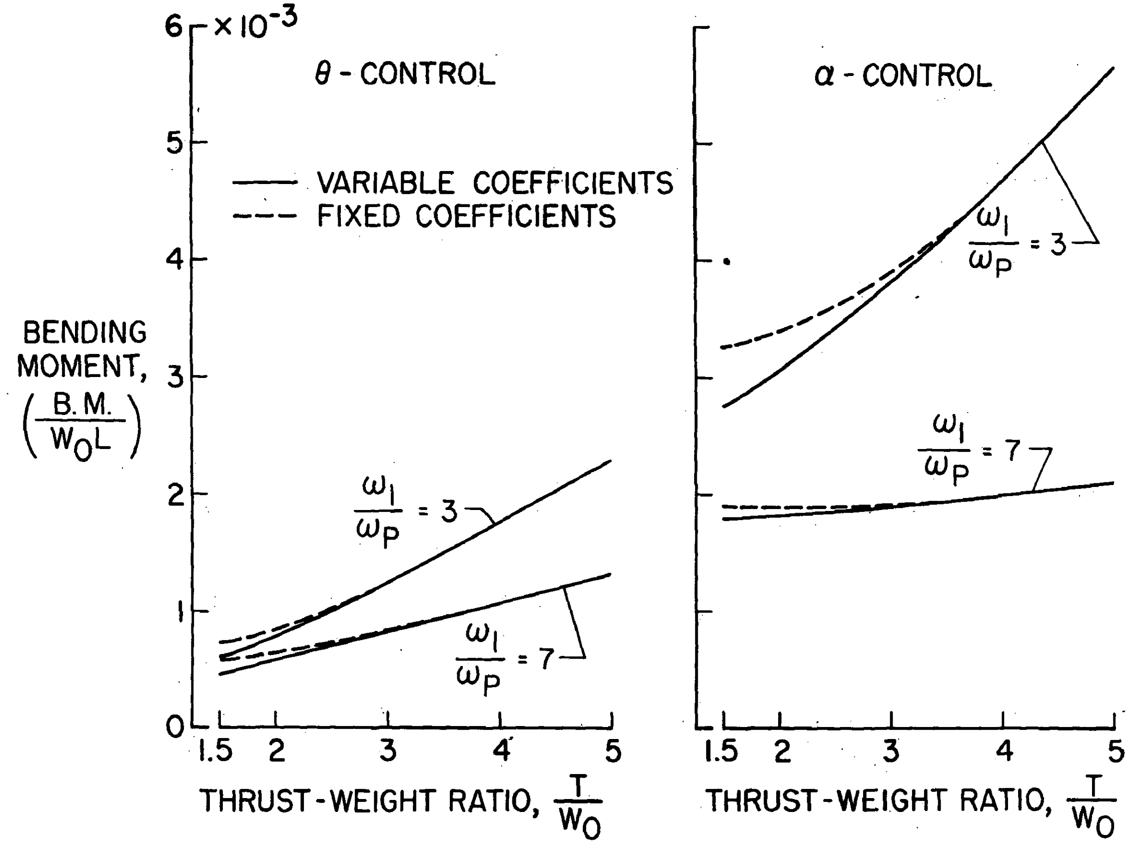

Figure 5.- Maximum bending-moment variation with thrust-to-weight ratio. $x = 0.3$, $\Lambda = 10{,}000$ ft, $(V_w)_{max} = 80$ ft/sec.

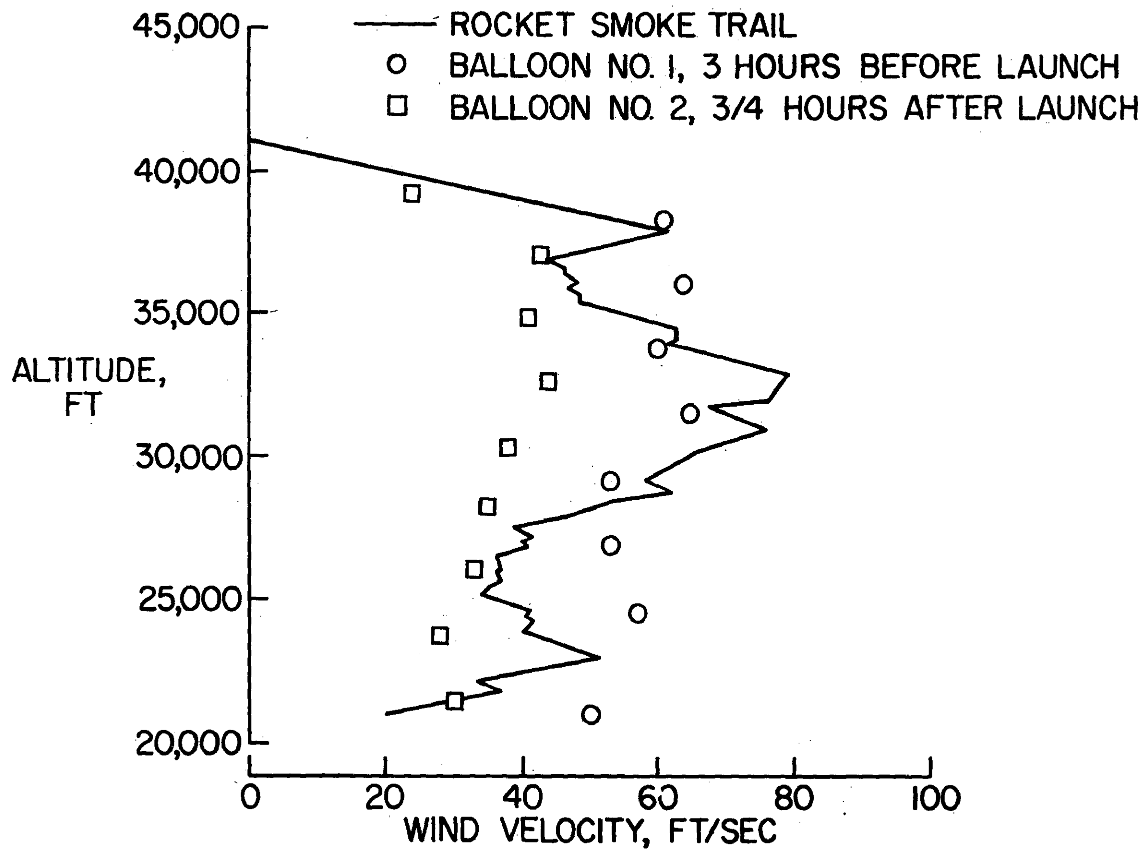

Figure 6.- Measured wind profiles (ref. 2).

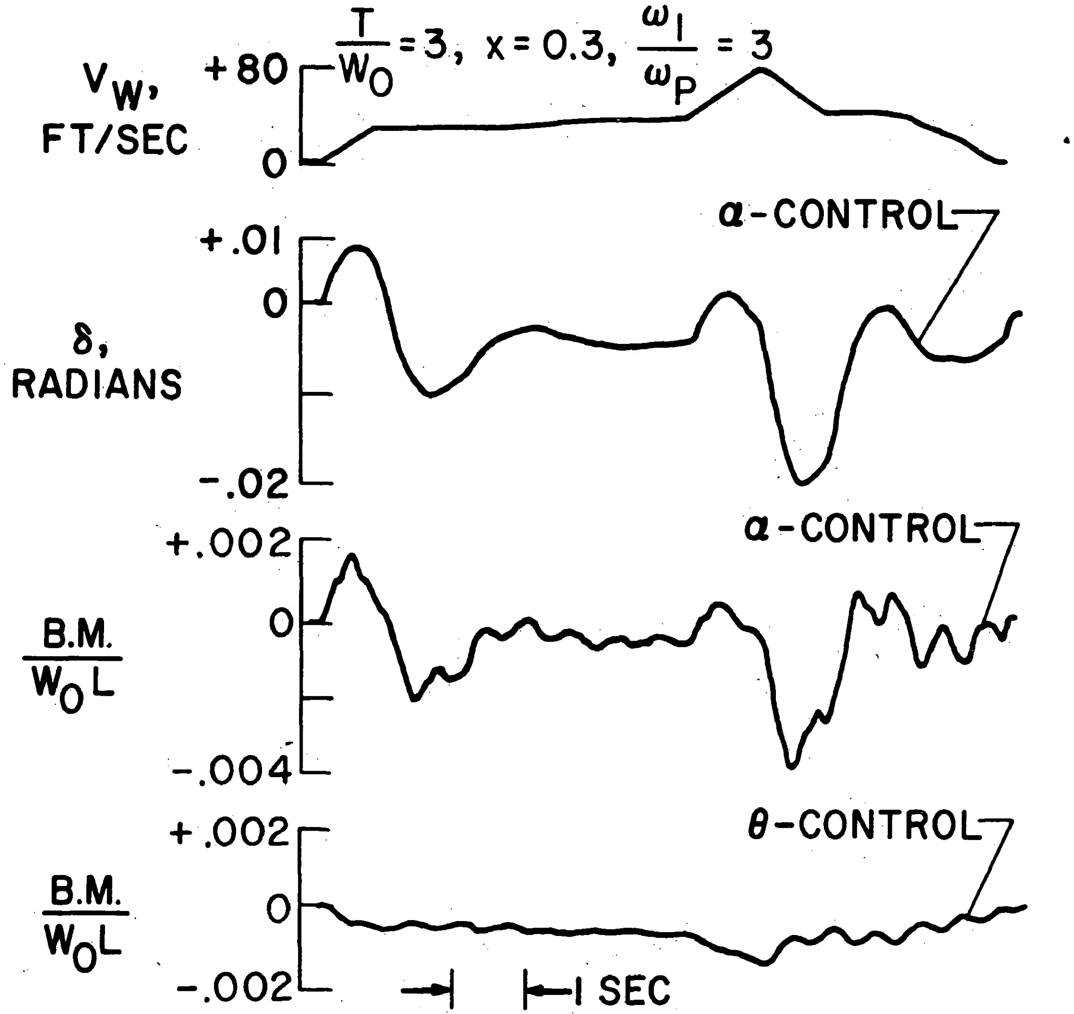

Figure 7.- Response time history due to flying through balloon wind profile no. 3.

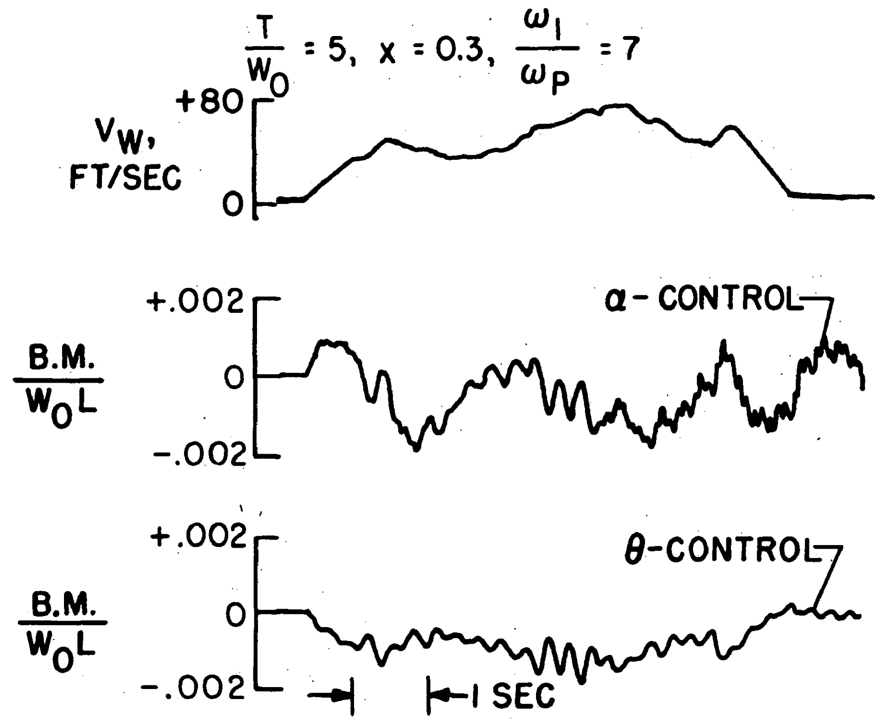

(a) α-control and θ-control.

Figure 8.- Bending-moment time histories due to flying through the smoke-trail wind profile.

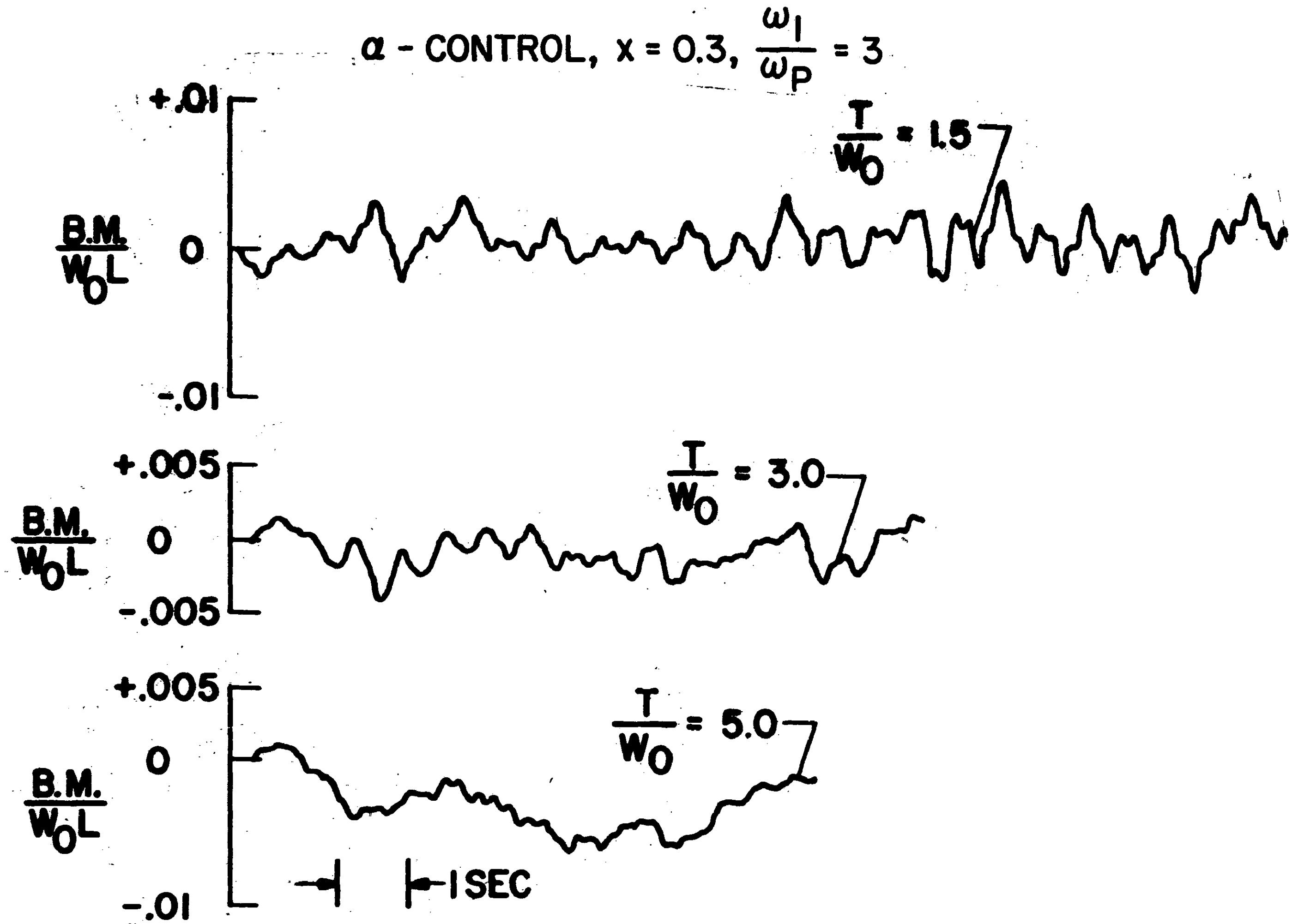

(b) Comparison at three thrust-to-weight ratios.

Figure 8.- Concluded.

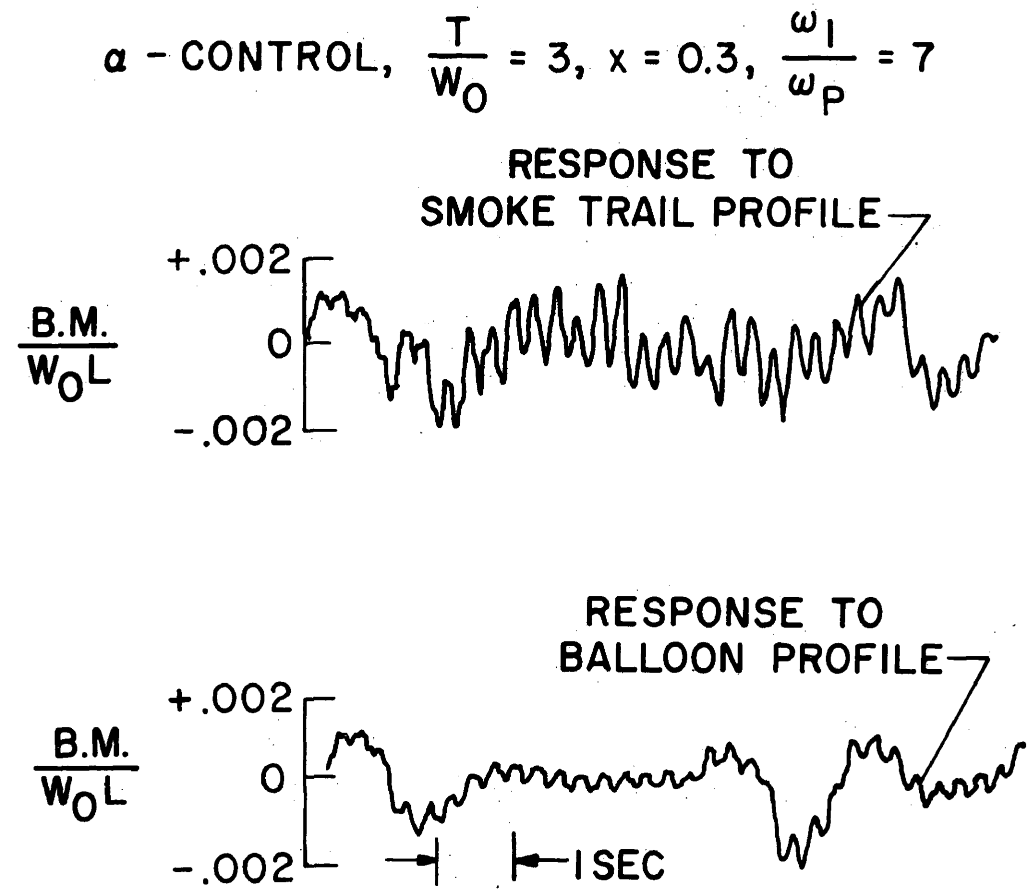

Figure 9.- Bending-moment time histories from flying through two wind profiles with α-control.

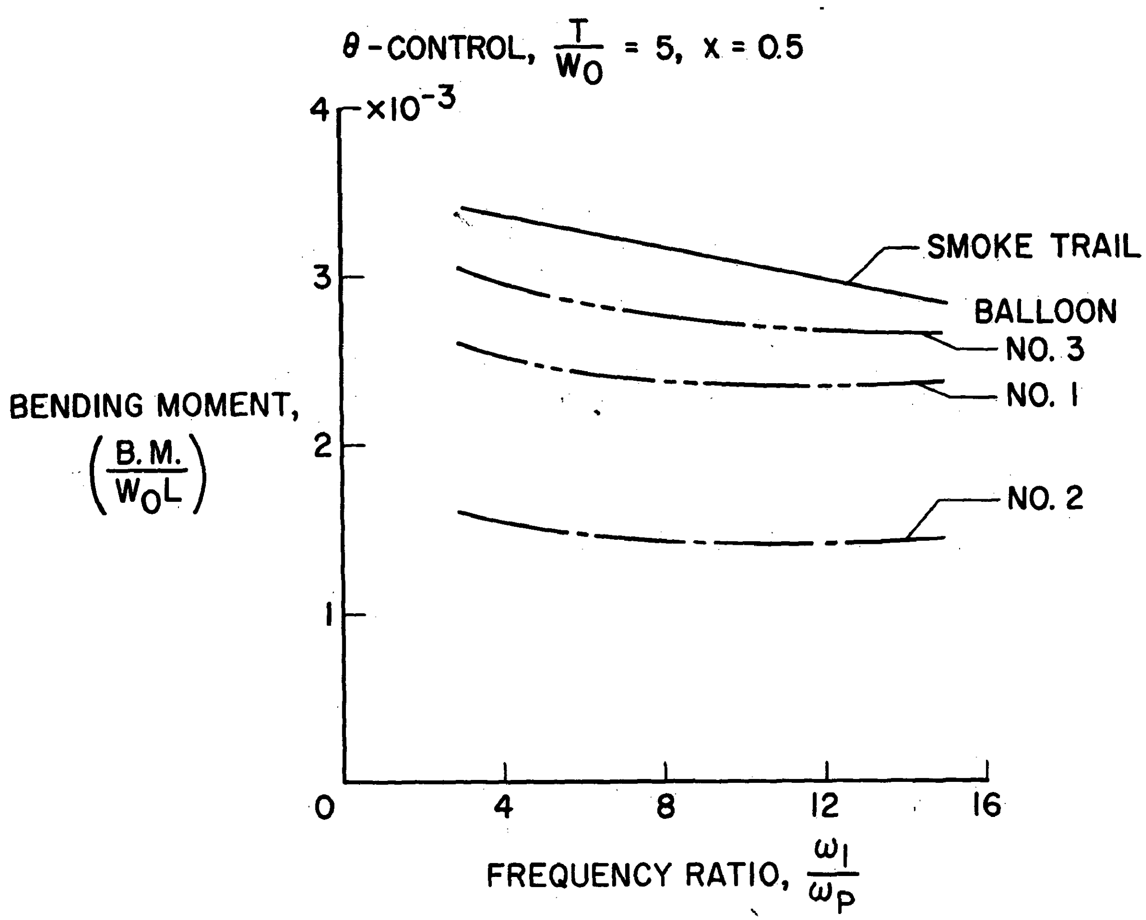

(a) θ-control.

Figure 10.- Maximum bending-moment variation with frequency ratio resulting from smoke-trail and balloon-measured wind profiles.

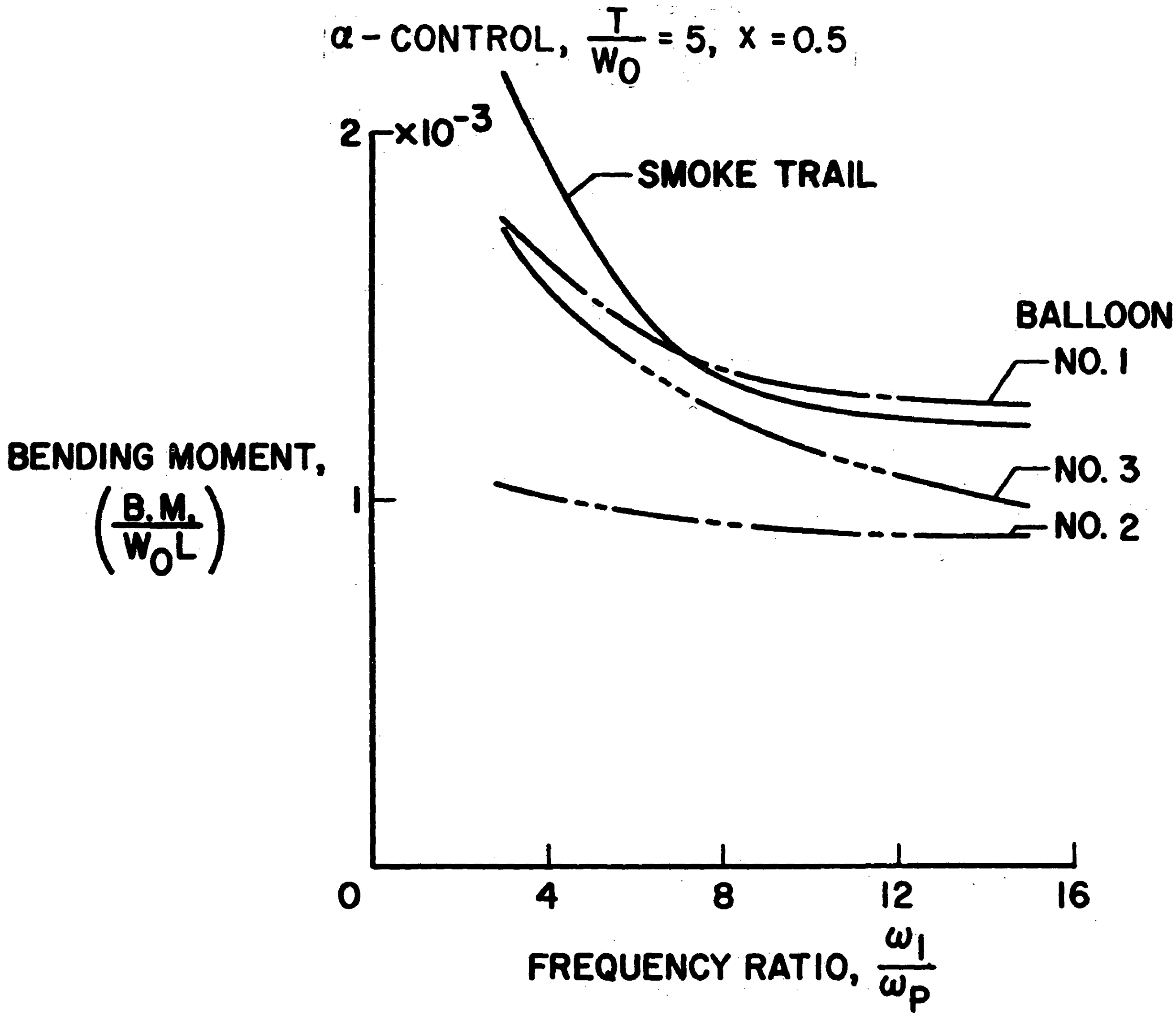

(b) α-control.

Figure 10.- Concluded.

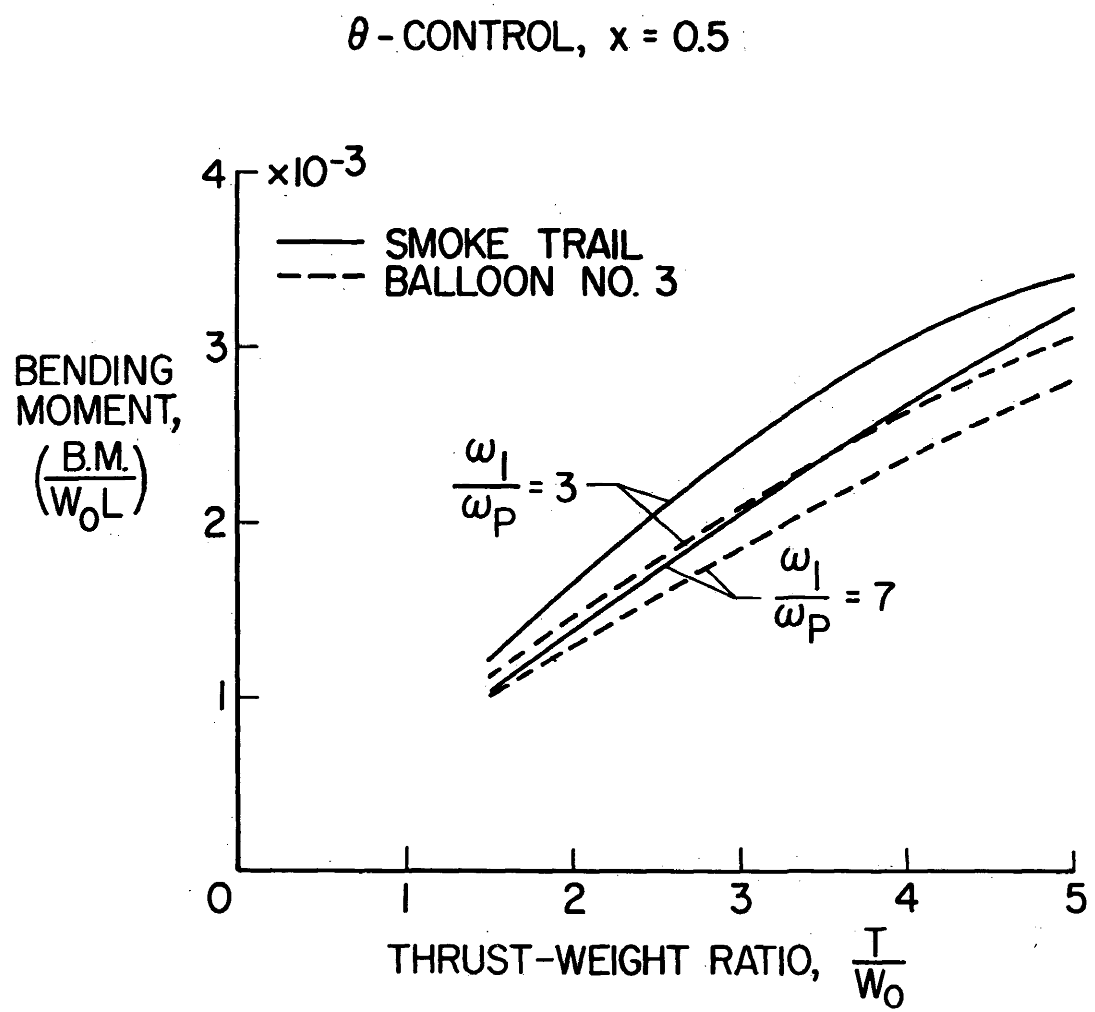

(a) θ-control.

Figure 11.- Maximum bending-moment variation with thrust-to-weight ratio resulting from smoke-trail and balloon-measured wind profiles.

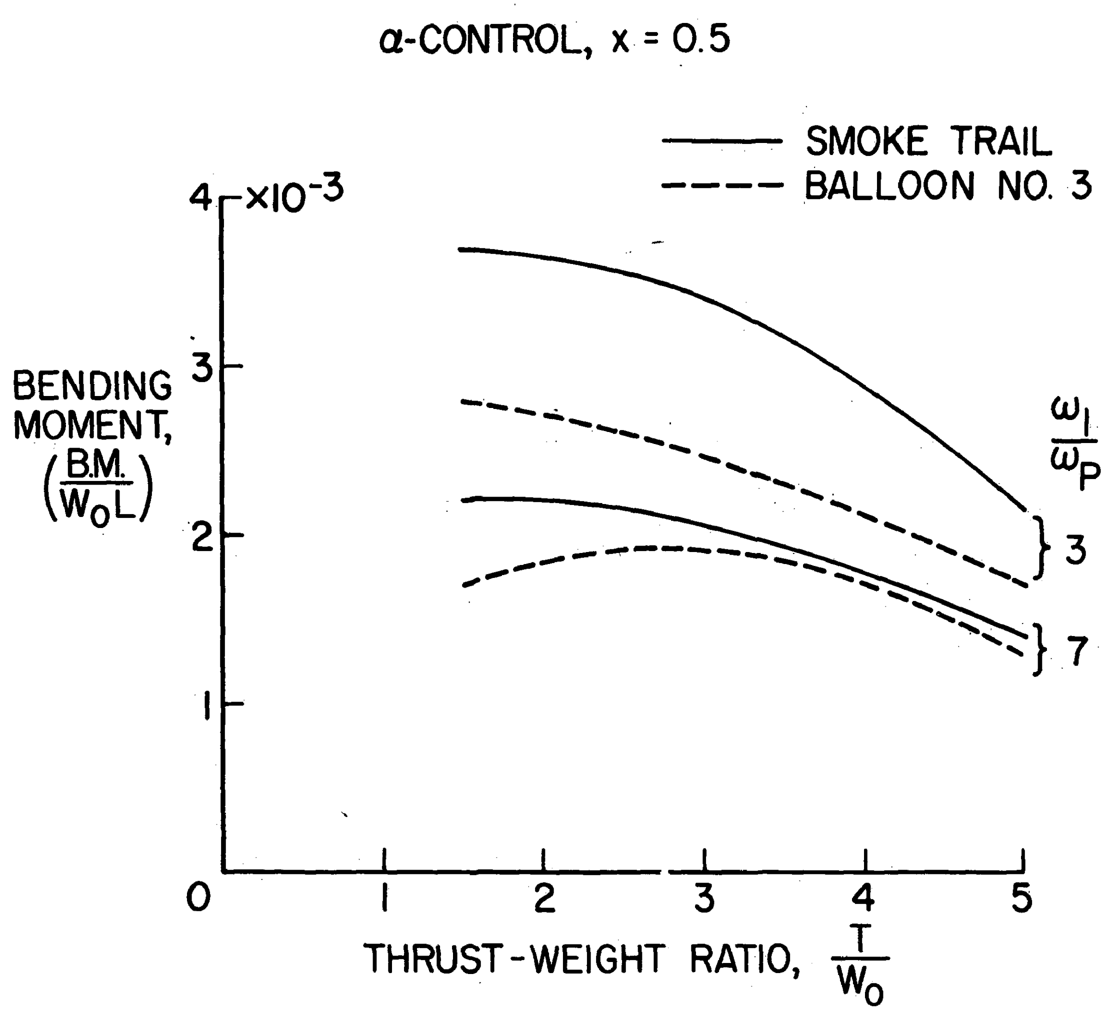

(b) α-control.

Figure 11.- Concluded.

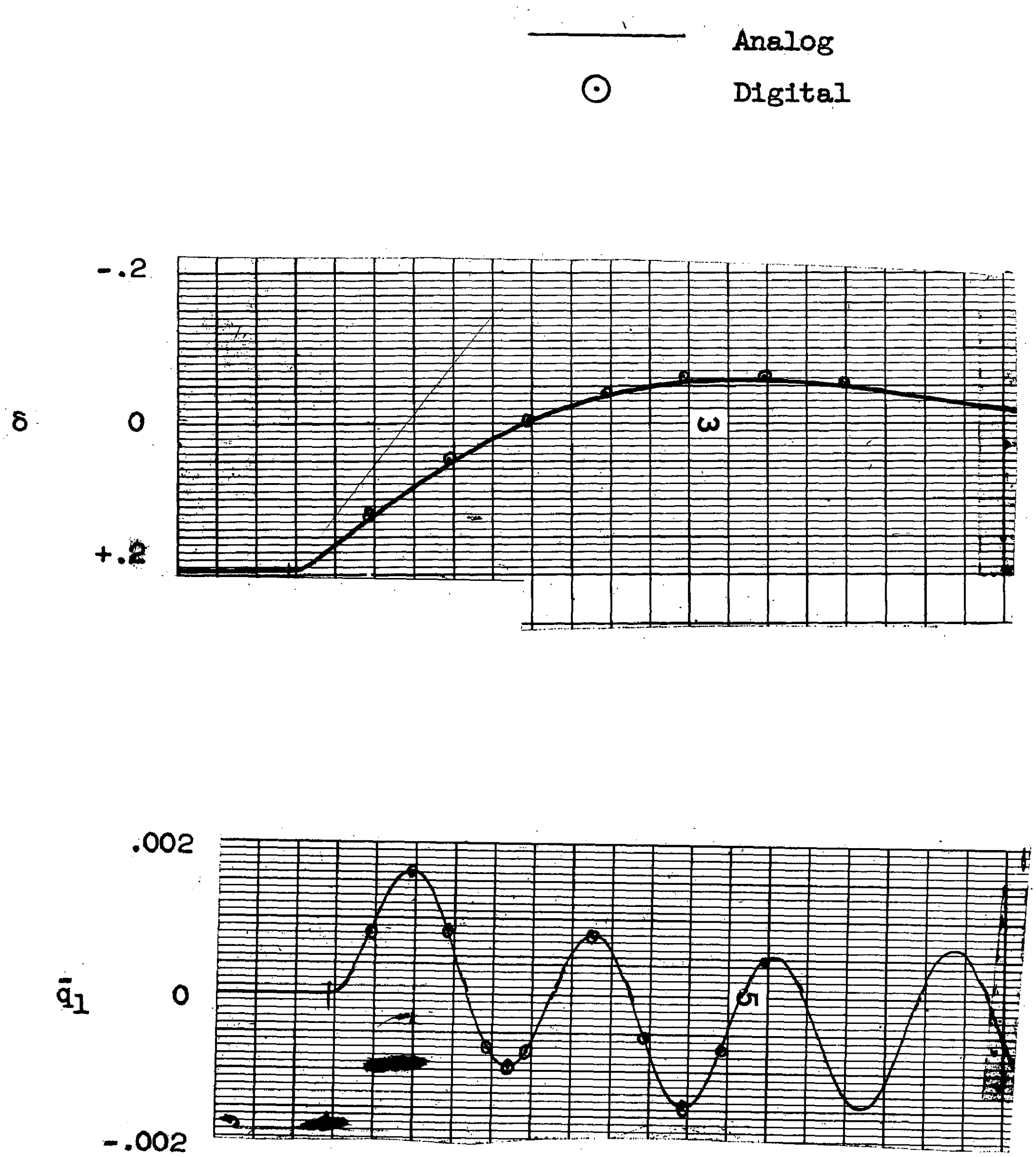

Figure 12.- Comparison of analog and digital time histories of engine deflection and first-mode deflection for step wind.

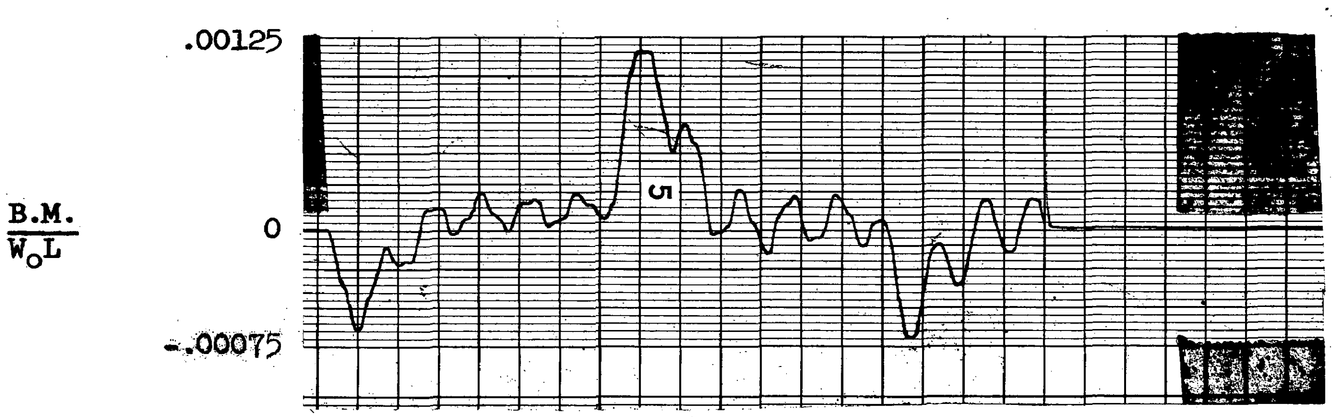

(a) Bending-moment time history due to flying through wind shear reversal. $x = 0.3$, $\Lambda = 10{,}000$ ft, $(V_W)_{max} = 40$ ft/sec, α-control.

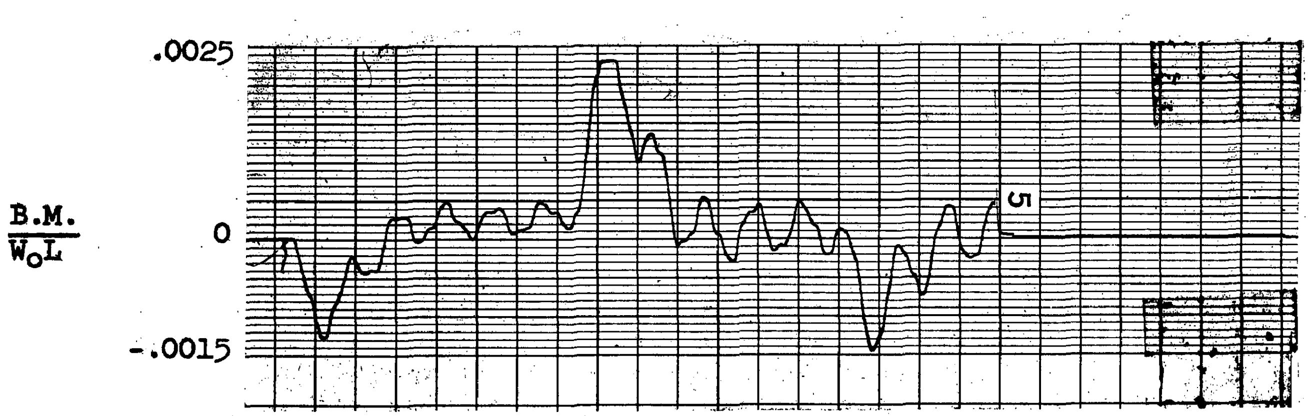

(b) Bending-moment time history due to flying through wind shear reversal. $x = 0.3$, $\Lambda = 10{,}000$ ft, $(V_W)_{max} = 80$ ft/sec, α-control.

Figure 13.- Demonstration of system linearity.